

NASA TM X-53298

July 21, 1965

G3/15 30390

TECHNICAL MEMORANDUM X-53298

A PRACTICAL APPROACH TO THE OPTIMIZATION OF THE SATURN V
SPACE VEHICLE CONTROL SYSTEM UNDER AERODYNAMIC LOADS

by

Robert S. Ryan and Dieter Teuber

George C. Marshall Space Flight Center
Huntsville, Alabama

ABSTRACT

The equations for the bending moment of a launch vehicle are written including the effects of bending and sloshing dynamics. By making certain simplifying assumptions, the bending moment equation is transformed to be a function of rigid vehicle angle of attack, engine deflection, bending mode acceleration and sloshing mode acceleration. This form is particularly advantageous for use in optimization techniques by the control engineer. The response of a Saturn V class vehicle was solved and the control system optimized to bending moments using data covering a period of six years, amounting to 4,384 measured wind profiles, and the GPS high speed repetitive analog computer. A comparison between the bending moment response envelope of the measured winds and the bending moment response of the MSFC synthetic wind profile is made.

NASA-GEORGE C. MARSHALL SPACE FLIGHT CENTER

TECHNICAL MEMORANDUM X-53298

July 21, 1965

A PRACTICAL APPROACH TO THE OPTIMIZATION OF THE SATURN V
SPACE VEHICLE CONTROL SYSTEM UNDER AERODYNAMIC LOADS

by

Robert S. Ryan

and

Dieter Teuber

DYNAMICS AND FLIGHT MECHANICS DIVISION
AERO-ASTRODYNAMICS LABORATORY

LIST OF ILLUSTRATIONS

<u>Figure</u>	<u>Title</u>	<u>Page</u>
1	Bending Coefficient for Engine Deflection,..... Angle of Attack	22
2	Bending Moment Coefficient for Bending Mode Dynamics.....	23
3	Bending Moment Coefficient for Sloshing Dynamics...	24
4	Coordinate System.....	25
5	Slosh Model.....	26
6	Bending Mode Deflection Curves.....	27
7	Control System Block Diagram.....	28
8	Complete GPS Facility.....	29
9-10	Details of the Computer.....	30-31
11	Schematic of a Typical Second Order Loop.....	32
12	Schematic for the Analog Simulation with Time Varying Parameters.....	33
13	Schematic for the Analog Simulation of Wind Profiles	34
14	Saturn V Configuration.....	35
15	Bending Moment vs. Probability of Exceedance.....	36
15A	Bending Moment vs. Probability of Exceedance.....	37
15B	Bending Moment Vs. Probability of Exceedance.....	38
16	MSFC Synthetic Profile.....	39
17	Angle of Attack vs. Probability of Exceedance.....	40
18	Engine Deflection vs. Probability of Exceedance....	41
19	Typical Response with Turbulence.....	42
19A	Typical Response without Turbulence.....	43

DEFINITION OF SYMBOLS

<u>Symbol</u>	<u>Definition</u>
a_0	position gain factor
a_1	rate gain factor
b_0	angle-of-attack gain factor
C_1	aerodynamic restoring force coefficient
C_2	control restoring force coefficient
$C_{Z\alpha f}$	normal force on fin
$C'_{Z\alpha}$	local normal force coefficient
D_0	reference diameter of vehicle
F_s	swivel engine thrust
\bar{g}	longitudinal acceleration
I	moment of inertia about c.g.
I_{corr}	correction of moment of inertia due to propellant oscillations
L_e	distance from gimbal point to c.g. of swivel engine
M	total vehicle mass
$M_{B\mu}$	generalized mass in vehicle bending
m_{fs}	slosh mass
M'	aerodynamic restoring moment
$m(x)$	local mass distribution
N'	aerodynamic normal force
Q	dynamic pressure times reference area
q	dynamic pressure

DEFINITION OF SYMBOLS (Continued)

<u>Symbol</u>	<u>Definition</u>
S	reference area
S_E	first moment of swivel engine about gimbal
V	vehicle velocity
V_w	wind velocity
X_{cg}	vehicle c.g.
X_k	point of bending moment
$X_E = X_T$	swivel point
X_{fs}	slosh mass location
X_v	angle-of-attack meter location
$\bar{X} = (X - X_{cg})$	bar indicates X station minus X_{cg}
$Y(x)$	bending mode deflection curve
$Y'(x)$	slope of bending mode deflection curve
α_w	wind angle V_w/V
β_c	engine command angle
β_E	thrust vector angle
ζ_B	structural damping
ζ_c	control mode damping
ζ_E	swivel engine damping
ζ_s	slosh damping
η_μ	generalized coordinate in bending
D_E	moment of inertia of swivel engine about gimbal

DEFINITION OF SYMBOLS (Continued)

<u>Symbol</u>	<u>Definition</u>
ξ_i	generalized coordinate of propellant oscillation
φ	generalized coordinate rigid body rotation
$\omega_{B\mu}$	natural frequency of body bending
ω_c	control frequency
ω_E	engine compliance frequency
ω_s	sloshing frequency

TECHNICAL MEMORANDUM X-53298

A PRACTICAL APPROACH TO THE OPTIMIZATION OF THE SATURN V SPACE VEHICLE CONTROL SYSTEM UNDER AERODYNAMIC LOADS

SUMMARY

The equations for the bending moment of a launch vehicle are written including the effects of bending and sloshing dynamics. By making certain simplifying assumptions, the bending moment equation is transformed to be a function of rigid vehicle angle of attack, engine deflection, bending mode acceleration and sloshing mode acceleration. This form is particularly advantageous for use in optimization techniques by the control engineer. The response of a Saturn V class vehicle was solved and the control system optimized to bending moments using data covering a period of six years, amounting to 4,384 measured wind profiles, and the GPS high speed repetitive analog computer. A comparison between the bending moment response envelope of the measured winds and the bending moment response of the MSFC synthetic wind profile is made.

INTRODUCTION

As a launch vehicle ascends through the atmosphere, it encounters many disturbances, the main one being wind velocity. Not only are the magnitudes of these wind velocities important, but also their rate of change. This leads to the consideration of wind magnitude, wind shear, and wind gust and turbulence. The reaction of the launch vehicle to these disturbances as it attempts to fly a specific flight trajectory produces an angle of attack which introduces loads on the vehicle structure. In order to properly size the vehicle structure and insure a successful flight with maximum payload capability, two important considerations in vehicle dynamics and control work are necessary: (1) A dynamic model is needed which will accurately describe the vehicle (including nonlinearities). This model should include the vehicle bending moment in a form suitable for control optimization techniques; also the wind input must include the wind magnitude, shear, and gust with a high level predictability. (2) Optimization techniques of the control system are needed that will reduce vehicle response to these disturbances, particularly, a reduction in the bending moment.

Many approaches have been used for representing the wind inputs and conducting response analyses. In general, these techniques make use of a rigid body representation of the vehicle flying through synthetic profiles. Responses obtained from gusts acting on an elastic vehicle are then superimposed on the wind loads to obtain total loads. At MSFC a synthetic wind profile approach has been taken that considers both wind magnitude, wind shear, and wind gust (Reference 1). Several other methods have been used for response prediction and have been evaluated in great detail by Avi-Dyne Research Inc. (Reference 2) under Air Force contract. In all these procedures, questions still arise since a high probability of not exceeding the design value is not guaranteed.

This paper presents a method for accurately describing the vehicle bending moment in terms of control system parameters. The wind input,

represented by a six-year sample of serially complete individual measured wind profiles (4,384), gives a reasonably accurate statistical representation of wind magnitude and wind shear. The wind speed profiles were measured by the standard GMD rawinsonde system. Finally, a high speed repetitive analog computer is used to run numerous control parameter variations. The control law is optimized to produce a minimum bending moment at one vehicle station. Also, the vehicle responses to these profiles are compared to those obtained from the MSFC synthetic wind profile.

The dynamic description of the launch vehicle, including wind inputs, is the first step in dynamic analysis. The second step is to describe response of the vehicle to wind inputs which establishes the control system gains that optimize some response value. It is felt that the best choice for this response value is the vehicle bending moment at some critical station. This choice was based on the facts that

- (1) the bending moment contains in some form all other pertinent response values and is therefore indicative of the overall vehicle response, and
- (2) by reducing the bending moment through the control system, additional payload could be obtained either by reducing structural weight or using lifting type trajectories.

Based on this choice of a parameter for optimizing the control gains, the basic procedures for analysis are formulated, and a special study of the Saturn launch vehicle is presented. A detailed development of the bending moment equation is discussed in the first section. The second section discusses the equations of motion and control equation. The third section discusses the high speed analog computer, while the fourth section deals with the wind input. The final section is an example study for Saturn V vehicle using the techniques presented.

ANALYSIS

Bending Moment Equation

Since the bending moment has been chosen as the parameter for optimizing the control system, a special discussion of the bending moment equation follows.

The two main approaches used to derive the bending moment equation are the mode displacement and mode acceleration, or direct method. Because of the simplicity of the form of the bending moment equation in the mode displacement method,

$$M_B(x_k, t) = \sum \eta_\mu(t) EI(x) Y''_\mu(x),$$

it would appear that this is the best form to use. However, after some studies were made using the equation in this form, it was found that several modes were needed for good convergence of the series and an accurate bending moment description. Also, little physical insight into the effect of the control system upon the bending moment could be visualized.

This led to the idea that the mode acceleration method would better describe the bending moment. The equation as used by stress engineers can be written, by neglecting small terms, as

$$M_B(x_k, t) = m'_{\alpha}(x_k) \alpha(t) + m'_{\beta}(x_k) \beta(t) + m'_{\tau}(x_k) \ddot{\tau}(t) + m'_{\phi}(x_k) \ddot{\phi}(t) \\ + \sum_{i=1}^m m'_{\xi}(x_k) \ddot{\xi}(t) + \sum_{\mu=1}^m m'_{\eta_\mu}(x_k) \ddot{\eta}_\mu(t).$$

Here, again, the effect of the control system parameters on the bending moment cannot be adequately analyzed. Also, mathematical errors are introduced easily since two numbers of near equal magnitude are subtracted to obtain the bending moment. Because it is desirable to have a form of the bending moment equation that to some extent circumvented the numerical errors and separated the various parameter effects, the equations of motion were substituted for lateral acceleration and angular acceleration into the bending moment equations, thus eliminating the rigid body acceleration terms. These rigid body equations are (by neglecting small terms)

$$\ddot{\phi}(t) = -C_1 \alpha(t) - C_2 \beta(t) + \sum_{i=1}^n \frac{m_i}{I} (x_i - x_{cg}) \ddot{\xi}_i(t) = 0$$

$$\ddot{\tau}(t) = k_2 \alpha(t) + k_3 \beta(t) - \sum_{i=1}^n \mu_i \ddot{\xi}_i(t).$$

Substituting these equations for the accelerations into the bending moment equations gives the final form of the bending moment equation as

$$\begin{aligned} M_B(x_k, t) = & M'_\alpha(x_k) \alpha(t) + M'_\beta(x_k) \beta(t) + \sum_{i=1}^n M'_{\xi i}(x_k) \ddot{\xi}_i(t) \\ & + \sum_{\mu=1}^m M'_{\eta \mu}(x_k) \ddot{\eta}_\mu(t). \end{aligned}$$

The bending moment equation in this form readily suits the needs of the control engineer for several reasons:

- (1) The various effects are completely separated, allowing insight into the problem. In particular, the trade-off between the effects of angle of attack and engine deflection is apparent, indicating the area of emphasis for the control law.
- (2) Nonlinear aerodynamic effects are more easily incorporated into the bending moment since only the M'_α term contains aerodynamic effects.
- (3) Each coefficient satisfies the boundary conditions of zero moment at each end, allowing better numerical flexibility and accuracy.

- (4) The coefficients are computed as by-products of the aerodynamic force and vibration programs and become only additional load-in values in the response programs.

Typical plots of these coefficients are shown in Figures 1 through 3. The ratio of $M'\alpha/M'\beta$ is shown on Figure 1. Here, it is obvious that the effective trade-off between α and β is always less than one, indicating that only a small percentage of load relief can be achieved through vehicle control laws.

Equations of Motion

To derive the equations of motion of the vehicle, a coordinate system having its origin at the center of gravity of the vehicle is chosen (Figure 4). The translation of this coordination system is eliminated by replacing it with an equivalent gravitational field. The rotation of the coordinate system in space is neglected. Since the vehicle is assumed to be symmetrical, no cross coupling is present; therefore, a planar analysis is applicable.

The vehicle is assumed to be controlled by an autopilot. The control force is obtained by swiveling the engines to produce a side force.

The liquid propellant dynamics is represented by an equivalent mechanical model consisting of an assembly of springs, dashpots, masses, and inertial discs arranged in such a manner as to represent the dynamic behavior of the moving liquid (Figure 5). This model exactly duplicates the forces and moments determined from the hydrodynamic solution and accurately reproduces the oscillating fluid, insofar as the assumptions made for the hydrodynamic solution are valid, viz, an incompressible, irrotational fluid with only small disturbances being admitted.

The aerodynamic forces are quasi-steady, based on normal force distributions measured or calculated along the longitudinal axis and the local angle of attack. Since all gust penetration effects have been found to be small for this vehicle configuration, they are neglected.

The bending effects of the launch vehicle structure are approximated by the superposition of several free-free normal mode shapes by

$$y(x,t) = \sum_{\mu=1}^n \eta_{\mu}(t) Y_{\mu}(x),$$

which defines the displacement of the vehicle centerline (Figure 6). The normal modes are computed with the swiveling engine masses removed. The liquid propellant mass is included in the bending mode calculations.

Based on these assumptions, Lagrange's equation is applied and the equations of motion derived, which include elastic body deflection, propellant oscillations, rigid body translation, rigid body rotation, and engine compliance. Additional equations are included for the dynamics of the control sensors. A complete set of these equations is given in the appendix.

The control system itself can be visualized in many forms depending on the designer's choice of elements, etc. Only one of this large number of possible systems is considered for this paper. This system consists of a gimbaling thrust vector produced by a hydraulic actuator activated by an electrical signal which has its source in a position gyro, rate gyro and angle-of-attack meter. By attaching proper gains to the three signals and summing, the command signal to the actuator is achieved. Additional control signal alterations can be achieved by using network filters to add damping to the bending modes (see Figure 7).

The control system used in this analysis is simplified somewhat by assuming that no filters are included. Bending mode stability is achieved by locating the rate gyros at the vehicle tail. It is assumed that the actuator dynamics can be represented by a second order system; therefore, the final control law becomes

$$m_2 \ddot{\beta}_c + m_1 \dot{\beta}_c + \beta_c = a_0 \phi_i + a_1 \dot{\phi}_i + b_0 \alpha_i$$

where

- ϕ_i is the indicated vehicle position,
- $\dot{\phi}_i$ is the indicated vehicle position rate, and
- α_i is the indicated angle of attack.

Using this type of the control equation allows some load reduction since angle-of-attack feedback is included. The trade-off in load reduction by using this angle-of-attack feedback will be the basis for the actual response study.

Computer Program and Wind Inputs

The basic philosophy of the technique as presented in this paper is to compute the response of the vehicle using many individual wind profiles. For each set of these many response runs on the computer, various combinations of the control gain settings are to be used to obtain the best setting in terms of reduced bending moment. By using this large sample of wind data and many control parameter variations, a high probability of prediction can be made. To facilitate the task of computing a large number of response runs, a high speed repetitive analog computer was chosen to solve the system of equations.

The electronic analog computer chosen is the General Purpose Simulator manufactured by GPS Instrument Co. in Massachusetts, which is well suited for the task of delivering in a short time thousands of solutions of the vehicle response. By time transformation, the events on the analog computer takes place 3000 times faster than in real time. One complete run does not exceed 150 m sec since there is an integration factor of 3000 sec^{-1} with a maximum of 50 volts from the amplifiers in repetitive operation. Thus, during one second, up to 20 solutions can be obtained from the take-off to cutoff of the launch stage at about 144 seconds. Because of the high-speed operation, the amplifiers have a bandwidth of 1 MHz , and the phase shift in the working range between 0 and 20 KHz amounts to less than 1 degree.

Figure 8 shows the complete GPS facility. The basic computing units contain about 50 integrators, 50 summing amplifiers, 350 coefficient potentiometers, 20 quarter-square multipliers and 15 function generators together with 70 amplifiers. Time-varying coefficients such as aerodynamic parameters or stochastic inputs can be fed, fully synchronized with the problem run, into the analog computer from two tape units. Each contains seven tracks. A tape speed of 60 inches/second guarantees satisfactory reproduction of the variable time functions. Solutions may also be recorded on these tapes. After an analog-digital conversion, the solutions may be further processed on a digital machine.

Furthermore, for statistical investigations, there are noise generators, switches, counters, comparators, probability distribution analyzers and adjustable filters. Besides the tape units, there are 17-inch oscilloscopes and a Honeywell "Visicorder" (Figures 9 and 10 show details of the computer).

It is a decided advantage of the repetitive operation that the total solution becomes immediately visible on an oscilloscope. Thus, the effect of varying certain state variables for optimization purposes becomes obvious at once.

All events on the computer, during repetitive operation, are controlled from one master generator providing the synchronizing pulses.

The equations for simulation of a launch vehicle on the GPS analog computer can be described by a system of linear differential equations with time-varying coefficients in the form (see appendix)

$$\begin{bmatrix} M(t) \end{bmatrix} \ddot{X} + \begin{bmatrix} C(t) \end{bmatrix} \dot{X} + \begin{bmatrix} K(t) \end{bmatrix} X = \left\{ q(t) \right\},$$

where $[M(t)]$, $[C(t)]$, and $[K(t)]$ are time-varying matrices, (X) the state vector and $q(t)$ generalized forces. These equations have to be supplemented by the control equation which connects the engine deflection with the state vector. The second derivatives of some variables appear in equations for second derivatives of other variables. This may lead to instabilities in the analog computer simulation because of closed algebraic loops. The loops contain summing amplifiers only and tend to oscillate at certain gain values. These difficulties were originally bypassed by a matrix transformation:

$$\ddot{X} = - [M(t)]^{-1} [C(t)] \dot{X} - [M(t)]^{-1} [K(t)] X + \{q(t)\} [M(t)]^{-1}.$$

Thus, equations are obtained containing the second derivative of one variable each. Figure 11 shows the simulation of one of 12 differential equations that are created by the elimination of other second derivatives.

A disadvantage of eliminating other second derivatives is the fact that, by the matrix transformation, new coefficients are generated that are sums and products of the old coefficients. Thus, we lose the ease of directly changing coefficient values on the analog computer that are in the original equations representing values such as thrust or mass. For this reason, a direct simulation of the original equations with time-varying coefficients was tried on the GPS as shown on Figure 12. No difficulties were encountered on the analog computer provided the variation of coefficients was not too far from "nominal" values. For variation of parameters in wide limits, however, for the sake of stability, all closed algebraic loops must be eliminated.

The final problem in vehicle response analysis is the representation of the disturbance or forcing function. The importance of the disturbance is obvious since any optimization of the control gains is a direct function of the disturbance. By nature, these disturbances are individually arbitrary. By the principles of statistics, a description of these disturbances can be made by probability density functions, by their power spectral density, and by correlation functions. However, these methods fail if applied to

nonlinear time-varying differential equations as they describe the behavior of the vehicle. On the analog computer, an investigation of these systems can be made without difficulty. It is therefore necessary to accurately simulate the statistical inputs together with the systems equations.

There are two ways of generating wind as a statistical input. One approach uses a magnetic tape which stores actually measured wind profiles up to an altitude of 27 km. The data were measured at Cape Kennedy by radar tracking of rising balloons, and are the Standard GMD rawinsonde winds. The high speed of the analog computer GPS in repetitive operation makes it feasible to feed the individual wind profile measurements of several years as inputs to the program and to evaluate the results statistically. Thus, results can be obtained for the behavior of the launch vehicle to individual measured wind profiles. The variables of interest such as engine deflection, angle of attack, or bending moment during flight can be registered on the analog computer if a preset limit has been exceeded. The number of exceedances of various limits can be related to the total number of wind profiles that have been used. In this way, the probability of exceeding a given value may be obtained.

Also of importance is the continuous and repetitive run of a specific wind profile on a closed magnetic tape. Certain control parameters may be varied with the goal of optimizing the response of certain variables and to establish a good compromise between often contradicting design criteria.

Optimization of transients for a specific wind profile does not necessarily mean that the behavior of the vehicle will be satisfactory for all winds that are likely to occur after take-off. Thus, a second method can be used for generating wind as a statistical input to the dynamic equations. The wind is generated by the method indicated on Figure 13. The output of the noise generator represents a random function described as "white noise." The bandwidth of constant power density is wider than the bandwidth of the

analog simulation. The wind is now considered to be the sum of three elements: a monthly mean value, a daily variation, and turbulence. Although this delineation is to quite an extent arbitrary, it is useful for reasons of practical wind measurements and for an electronic synthesis, whereby each element can be changed independently from the other. The monthly mean is duplicated from a function generator; daily variation and turbulence are filtered out from the white noise by two time-varying filters. The bandwidth of the filters F_W and F_T is increased with increasing vehicle velocity. Zero-crossing intervals, distribution and exceedances in the time-varying functions are determined or can be changed by the filter parameters ζ and ω .

Although both procedures for generating wind inputs can be used, this study used a variation of the two. First, the vehicle response was studied using the individual rawinsonde winds. As a follow-on study the standard rawinsonde winds had turbulence superimposed by filtering the white noise generator output. The turbulence spectrum superimposed on the rawinsonde measured profiles had a variance of approximately $1.5 \text{ m}^2/\text{sec}^2$. A separate spectrum was generated and superimposed on each profile. A profile showing the rawinsonde with superimposed turbulence is shown in Figure 19.

Although this model for the turbulence may not be completely representative, it serves as the best model available and these wind profiles should give representative answers of the effects of turbulence on vehicle response. At the present time, individual detailed wind profiles are being obtained; however, a sufficient number have not yet been collected for a good sample. Once these data are available in representative quantity, the above winds will be replaced.

APPLICATION TO SATURN V LAUNCH VEHICLE

The technique for conducting a vehicle response to inflight winds and optimizing the control law to minimize the bending moment was applied to the Saturn V launch vehicle (Figure 14). To conduct the study, the bending moment value occurring at the vehicle c.g. was used as the response value.

The basic parameters chosen for varying were the control gains a_0 and b_0 . First, the sum of the gains are chosen, thereby choosing the rigid body control frequency, as

$$a_0 + b_0 = \text{constant.}$$

Then for each value of c the ratio of b_0/a_0 is varied from zero to a large number.

This study was carried out using constant flight conditions. The time chosen for freezing the flight conditions was maximum loading. By freezing the flight conditions at 70 seconds flight time, the vehicle is flown along the total wind profile at a constant velocity, reaching the corresponding altitude and flight time conditions. Considering the vehicle behavior in this fashion should lead to a conservative value since the early part of the trajectory has larger dynamic pressure than would be experienced in actual flight. Future studies will eliminate this assumption by using time varying coefficients.

Examples of the response results of vehicle bending moment are shown on Figure 15. The ratio of the number of times the bending moment exceeds a preset limit to the total number of wind profiles is plotted. As indicated on the plots in Figure 15, the gain ratio b_0/a_0 was used as parameter. It is obvious that a gain setting of $a_0/b_0 = 1.5$ produces the lowest bending moment response.

The effect of adding turbulence to the rawinsonde wind profiles can also be seen on Figures 15, 17, and 18. Adding turbulence increases the number of exceedances and slightly changes the optimum gain setting. Also indicated on Figure 15 as straight lines are the bending moment values obtained using the MSFC synthetic profile (Figure 16). This synthetic profile is the MSFC 99 percent wind shear, 95 percent wind magnitude profile. The quasi-steady state wind speeds are not expected to be exceeded by the given percentage of time based on the windiest month. It can be

seen from the plot that the synthetic profile produces a bending moment value that will not be exceeded more than 3 percent of the time for the windiest month or 0.7 percent for the total number of winds run. Since this profile was designed for 95 percent wind magnitude during the windiest month, the profile gives realistic response results.

Typical plots of the engine deflection, and angle-of-attack exceedance ratios plotted vs amplitude are shown on Figures 17 and 18. Also, the synthetic profile results are included as straight lines.

To further illustrate the technique, Figure 19 is a typical set of response values obtained when the bending moment exceeded a preset limit. By capturing this wind on a tape loop, the bending moment response is displayed on the oscilloscope by changing the control gains in an attempt to reduce the moment. Additional information is recorded by photographing a series of individual bending moment responses to the individual winds. Figure 20 is an envelope of these bending moment responses to the individual winds for February 1958.

CONCLUSIONS

The technique of using the high speed repetitive analog computer to study the response of a launch vehicle to a large sample of individual winds is a valuable tool, since large samples can be run using winds that have high frequency components. This adds greatly to the assurances of the predicted loads.

Since the speed of the computer is very fast, the optimization of the control law using this large sample of winds is feasible. The use of the bending moment for this optimization parameter is a logical choice for a practical approach to the vehicle design. The method as presented should be a valuable design tool, adding flexibility and reliability to vehicle design.

APPENDIX

Aerodynamic Coefficients

$$B_{ij} = \frac{1}{4D_0} \int_{-L/2}^{L/2} C'_{Z\alpha}(x) Y_i(x) Y_j(x) dx + \frac{1}{4} C_{Z\alpha f} Y_i(x_f) Y_j(x_f)$$

$$C_{ij} = \frac{1}{4D_0} \int_{-L/2}^{L/2} C'_{Z\alpha}(x) Y_i(x) Y'_j(x) dx + \frac{1}{4} C_{Z\alpha f} Y_i(x_f) Y'_j(x_f)$$

$$D_{i \text{ or } j} = \frac{1}{4D_0} \int_{-L/2}^{L/2} C'_{Z\alpha}(x) Y_j(x) dx + \frac{1}{4} C_{Z\alpha f} Y_j(x_f)$$

$$\bar{D}_{i \text{ or } j} = \frac{1}{4D_0} \int_{-L/2}^{L/2} C'_{Z\alpha}(x) Y_j(x) \bar{X}(x) dx + \frac{1}{4} C_{Z\alpha f} Y_j(x_f)$$

$$E_i = \frac{1}{4D_0} \int_{-L/2}^{L/2} C'_{Z\alpha}(x) Y'_j(x) dx + \frac{1}{4} C_{Z\alpha f} Y'_j(x_f)$$

$$\bar{E}_i = \frac{1}{4D_0} \int_{-L/2}^{L/2} C'_{Z\alpha}(x) Y'_j(x) \bar{X}(x) dx + \frac{1}{4} C_{Z\alpha f} Y'_j(x_f) \bar{X}(x_f)$$

$$F_k = \frac{1}{4D_o} \int_{-L/2}^{L/2} C'_{Z\alpha}(x) \bar{X}^k dx + \frac{1}{4} C_{Z\alpha f} \bar{X}_f^k \quad k = 0, 1, 2$$

$$C_1 = \frac{2Q F_o}{I} \quad C_2 = \frac{F_s \bar{X}_E}{I}$$

$$K_1 = \bar{g} \quad K_2 = \frac{2Q F_o}{m} \quad K_3 = F_s/m$$

Bending Moment Coefficients

$$M'_{\alpha} = \frac{q_s}{D_o} \int_{x_T}^{x_k} C'_{Z\alpha}(x_k - x) dx - \frac{N'}{m} \int_{x_T}^{x_k} m'(x) (x_k - x) dx$$

$$- C_1 \int_{x_T}^{x_k} m'(x) (x_k - x) (x_{cg} - x) dx.$$

$$M'_{\beta} = F_s X_k - K_2 \int_{x_T}^{x_k} m'(x) (x_k - x) dx - \frac{F_s X_T}{I} \int_{x_T}^{x_k} m'(x) (x_k - x) (x_{cg} - x) dx$$

$$M'_{\xi_i} = \frac{m_{si}}{m} \int_{x_T}^{x_k} m'(x) (x_k - x) dx - \frac{m_{si}}{I} (x_{si} - x_{cg}) \int_{x_T}^{x_k} m'(x) (x_{cg} - x) (x_k - x) dx$$

$$- m_{si} (x_k - x_{si})$$

$$M_{\dot{\eta}_{\mu}}' = - \int_{x_T}^{x_k} m'(x) (x_k - x) Y_{\mu}(x) dx$$

Miscellaneous Definitions

$$\varphi_i = \varphi - \sum_{\mu=1}^n \eta_{\mu} Y_{\mu}'(x_{\varphi})$$

$$\dot{\varphi}_i = \dot{\varphi} = \sum_{\mu=1}^n \dot{\eta}_{\mu} Y_{\mu}'(x_g)$$

$$\alpha_i = \varphi - \frac{\dot{y}}{V} - \sum_{\mu=1}^n \eta_{\mu} Y_{\mu}'(x_{\alpha}) - \sum \frac{\eta_{\mu} Y_{\mu}}{V} (x_{\alpha}) - \frac{\bar{X}_{\alpha} \dot{\varphi}}{V} + \alpha_w$$

Control Frequency

$$\omega_c = \sqrt{(a_0 + b_0) C_1 + C_2}$$

Control Frequency Damping

$$2\zeta_c \omega_c = a_1 C_2$$

Rigid Angle of Attack

$$\alpha = \varphi - \frac{\dot{y}}{V} + \alpha_w$$

Equations of Motion

Translation

$$\begin{aligned}
 & \left(m + m_E + \frac{Q}{V^2} J_O \right) \ddot{y} - \frac{Q}{V^2} J_1 \ddot{\phi} + \left[S_E Y'_j(x_E) + M_E Y_j(x_E) \right] \ddot{\eta}_j \\
 & + M_{fs} \ddot{\xi}_s - S_E \ddot{\beta}_E + \frac{2Q}{V} F_O \dot{y} - \frac{2Q}{V} F_1 \dot{\phi} - \left[2QF_O + (m + m_E)g \right] \varphi \\
 & + \frac{2Q}{V} D_j \dot{\eta}_j + \left[QE_j + (m + m_E) \bar{g} Y'_j(x_E) \right] \eta_j - F_s \beta_E = \frac{2Q}{V} F_O V_w.
 \end{aligned}$$

Rotation

$$\begin{aligned}
 & (I - I_{corr}) \ddot{\phi} \left[- (\theta_E + S_E \bar{x}_E) Y'_j(x_E) - S_E Y_j(x_E) - m_E \bar{x}_E Y_j(x_E) \right] \ddot{\eta}_j \\
 & + m_{fs} \bar{x}_{fs} \ddot{\xi}_s + (\theta_E + S_E \bar{x}_E) \ddot{\beta}_E - \frac{2QF_1}{V} \dot{y} + \frac{2QF_2}{V} \dot{\phi} + 2QF_1 \varphi \\
 & + \frac{2Q}{V} \bar{D}_j \dot{\eta}_j - \left\{ m_E \bar{g} Y_j(x_E) + S_E \bar{g} Y'_j(x_E) - \varphi \bar{E}_j - (m + m_E) \bar{g} \right. \\
 & \left. Y_j(x_E) - \bar{x}_E Y'_j(x_E) \right\} \eta_j - m_{fs} \bar{g} \xi_s + (S_E \bar{g} + F_s \bar{x}_E) \beta_E \\
 & = - \frac{2Q}{V} (F_1 V_w).
 \end{aligned}$$

Bending

$$\begin{aligned}
& \left[m_E Y_i(x_E) + S_E Y_j'(x_E) \right] \ddot{y} + \left[-m_E (\bar{x}_E + l_E) Y_i(x_E) - Y_j'(x_E) (\theta_E + S_E \bar{x}_E) \right] \ddot{\phi} \\
& + \left\{ M_{Bi} + m_E Y_i(x_E) \left[L_E Y_j'(x_E) + Y_j(x_E) \right] + Y_i'(x_E) \left[\theta_E Y_j'(x_E) \right. \right. \\
& \left. \left. + S_E Y_j(x_E) \right] \right\} \ddot{\eta}_j + m_{fs} Y_i(x_s) \ddot{\xi}_s + \left[-S_E Y_i(x_E) - \theta_E Y_i'(x_E) \right] \ddot{\beta}_E \\
& + 2 \frac{Q}{V} D_i \dot{y} + 2 \frac{Q \bar{D}_i}{V} \dot{\phi} - \left[m_E \bar{g} Y_i(x_E) + S_E \bar{g} Y_i'(x_E) + 2 Q D_i \right] \varphi \\
& - \left[-2 \omega_{Bi} M_{Bi} \zeta_{Bi} + \frac{Q}{V} B_{ij} \right] \dot{\eta}_j + \left[-\omega_{Bi}^2 M_{Bi} - m_E \bar{g} Y_i(x_E) Y_j'(x_E) \right. \\
& \left. - m_E \bar{g} Y_i'(x_E) Y_j(x_E) - S_E \bar{g} Y_j'(x_E) Y_i'(x_E) + Q C_{ij} \right] \eta_i \\
& - \left[-\bar{g} m_{fs} Y_i'(x_{fs}) \right] \xi_s - \left[S_E \bar{g} Y_i'(x_E) + F_s Y_i(x_E) \right] \beta_E = 2 \frac{Q}{V} D_1 V_w.
\end{aligned}$$

Fuel Sloshing

$$\begin{aligned}
& \ddot{y} - \bar{x}_{fs} \ddot{\phi} + Y_j(x_{fs}) \ddot{\eta}_j + \ddot{\xi}_s - \bar{g} \varphi - \left[-\bar{g} Y_j'(x_{fs}) \right] \eta_j + \left[+2 \omega_{fs} \zeta_{fs} \right] \dot{\xi}_s \\
& + \omega_{fs}^2 \xi_s = 0.
\end{aligned}$$

Swivel Engine

$$\frac{S_E \ddot{y}}{\theta_E} + \frac{S_E \ddot{x}_E}{\theta_E} \ddot{\phi} + \left[Y'_j(x_E) - \frac{S_E Y_j(x_E)}{\theta_E} \right] \ddot{\eta}_j + \ddot{\beta}_E + \frac{S_E \ddot{g}}{\theta_E} \phi - \frac{S_E \ddot{g}}{\theta_E} Y'_j(x_E) \eta_j$$

$$+ 2\zeta_E \omega_E \dot{\beta}_E + \left(\omega_E^2 + \frac{S_E \ddot{g}}{\theta_E} \right) \beta_E - 2\zeta_E \omega_E \dot{\beta}_c - \omega_E^2 \beta_c = 0.$$

Control Equation

$$m_2 \ddot{\beta}_c + m_1 \dot{\beta}_c + \beta_c = a_0 \left[\phi - \sum_{j=1}^n Y'_j(x_\phi) \eta_j \right] + a_1 \left[\dot{\phi} - \sum_{j=1}^n Y'_j(x_g) \dot{\eta}_j \right]$$

$$+ b_0 \left[\phi - \frac{\dot{y}}{V} - \sum_{j=1}^n Y'_j(x_\alpha) \eta_j - \sum_{j=1}^n \frac{\dot{\eta}_j}{V} Y_j(x_\alpha) + \frac{\ddot{x}_\alpha \dot{\phi}}{V} + \frac{V_w}{V} \right].$$

Rate Gyro

$$\frac{\ddot{\theta}_i}{\omega_g^2} + \frac{2\zeta_g}{\omega_g} \dot{\theta}_i + \theta_i = \dot{\phi}_g = \dot{\phi} - \sum \dot{\eta}_v Y'_v(x_g).$$

α -Meter

$$\ddot{\alpha}_i + 2(\zeta_A + \zeta_m) \omega_\alpha \dot{\alpha}_i + \omega_\alpha^2 \alpha_i = \ddot{\phi} + \left(2\zeta_A \omega_\alpha + \frac{\ddot{x}_\alpha}{V} \omega_\alpha^2 \right) \dot{\phi}$$

$$- \sum (\ddot{\eta}_v + 2\zeta_A \omega_\alpha \dot{\eta}_v + \omega_\alpha^2 \eta_v) Y'_v(x_\alpha) - \frac{\omega_\alpha^2}{V} \sum \dot{\eta}_v Y_v(x_\alpha) - \frac{\omega_\alpha^2}{V} \dot{y}.$$

REFERENCES

1. Daniels, Glenn E., "Natural Environment (Climatic) Criteria Guidelines for Use in MSFC Launch Vehicle Development, 1963 Revision," MSFC, MTP-AERO-63-8, January 1963, Unclassified.
2. Hobbs, N. P., E. S. Criscione, and M. Ayvzzien, "Simplified Analytical Methods for Use in Preliminary Design of Vertically Rising Vehicles Subjected to Wind Shear Loads," FDL-TDR-64-8, Parts I and II, Prepared under Contract No. AF 33(657)-10185 by Avi-Dyne Research, Inc.

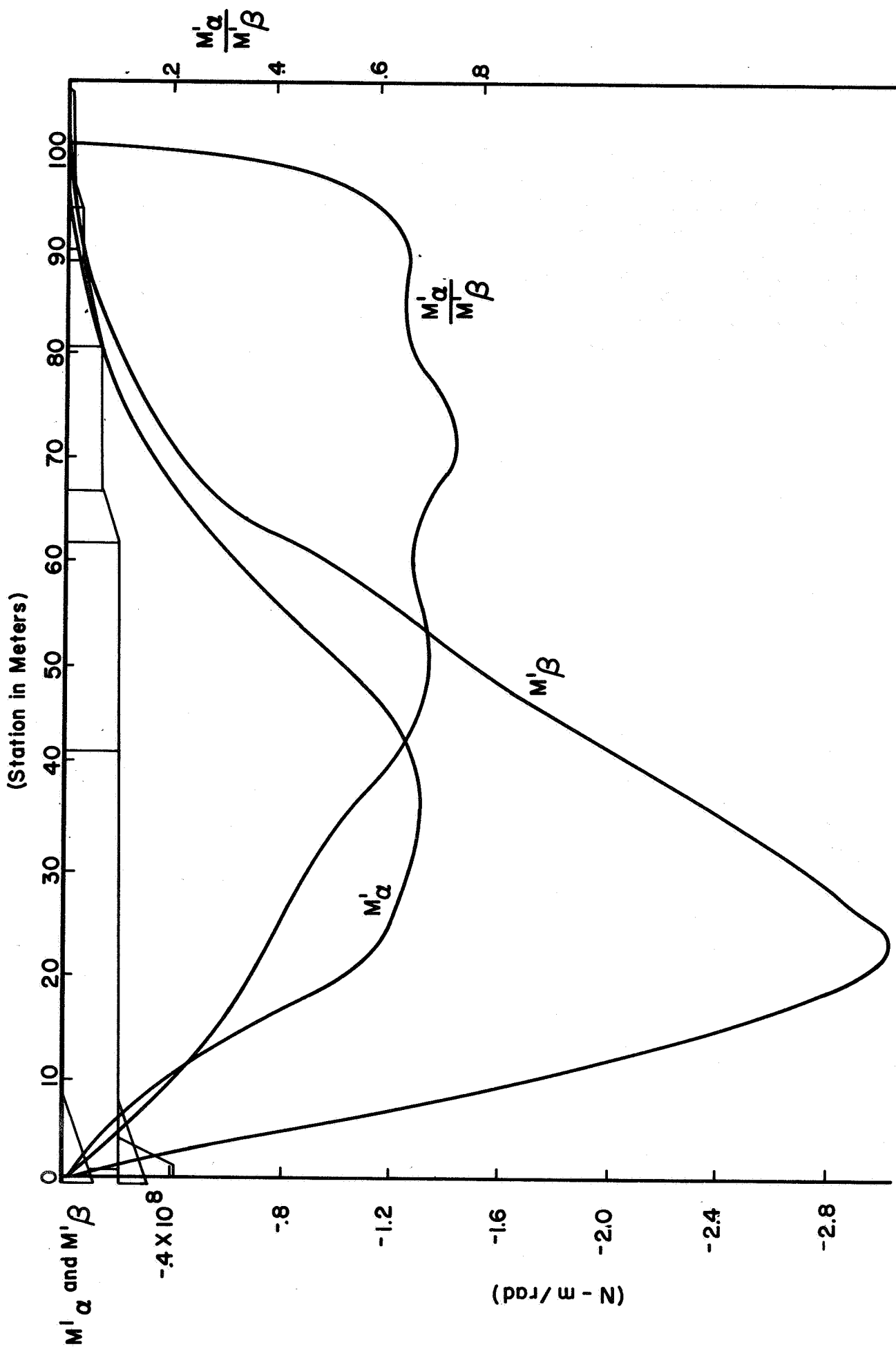


FIG.1 BENDING COEFFICIENT FOR ENGINE DEFLECTION ANGLE OF ATTACK

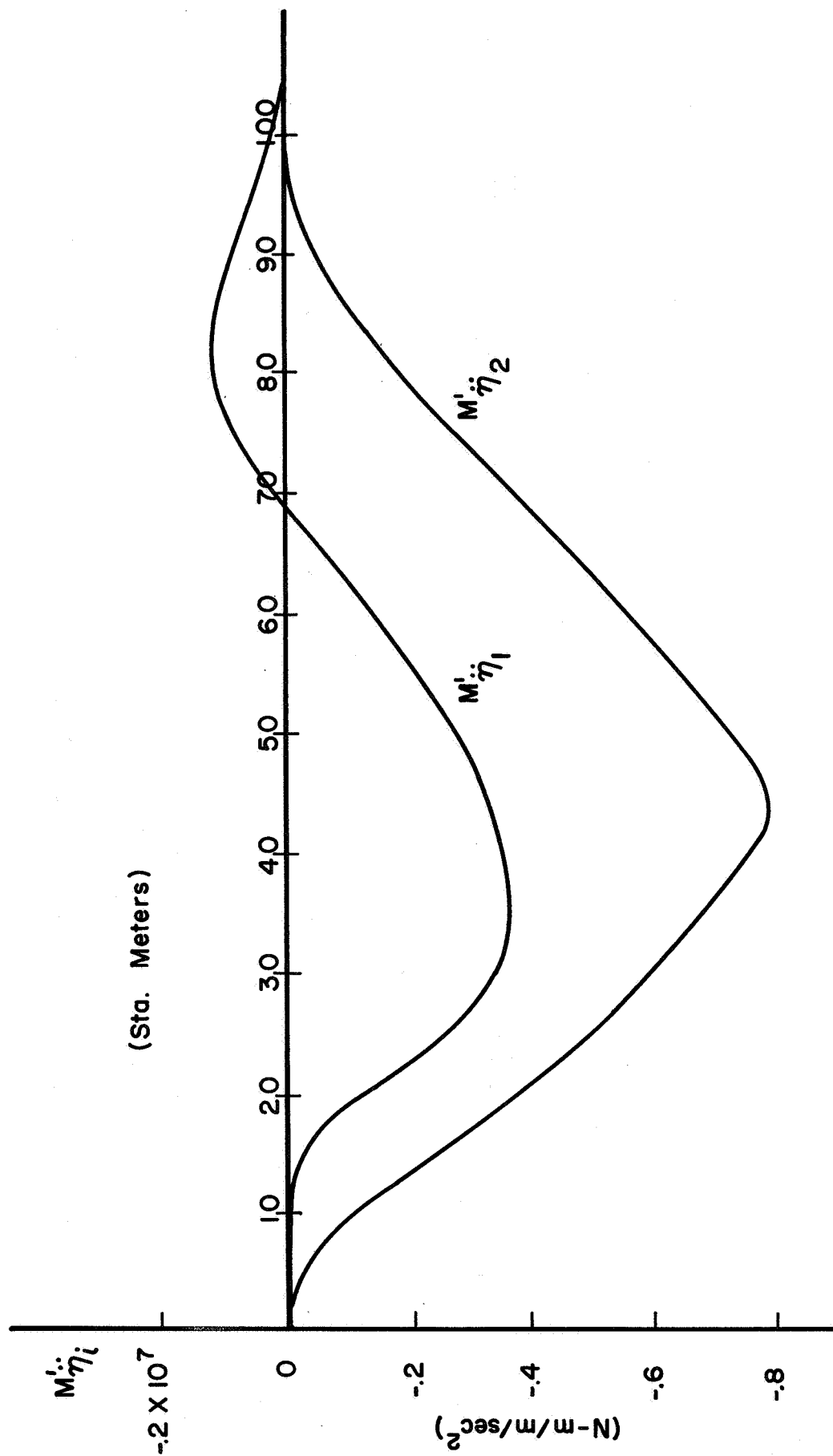


FIG 2 BENDING MOMENT COEFFICIENT FOR BENDING MODE DYNAMICS

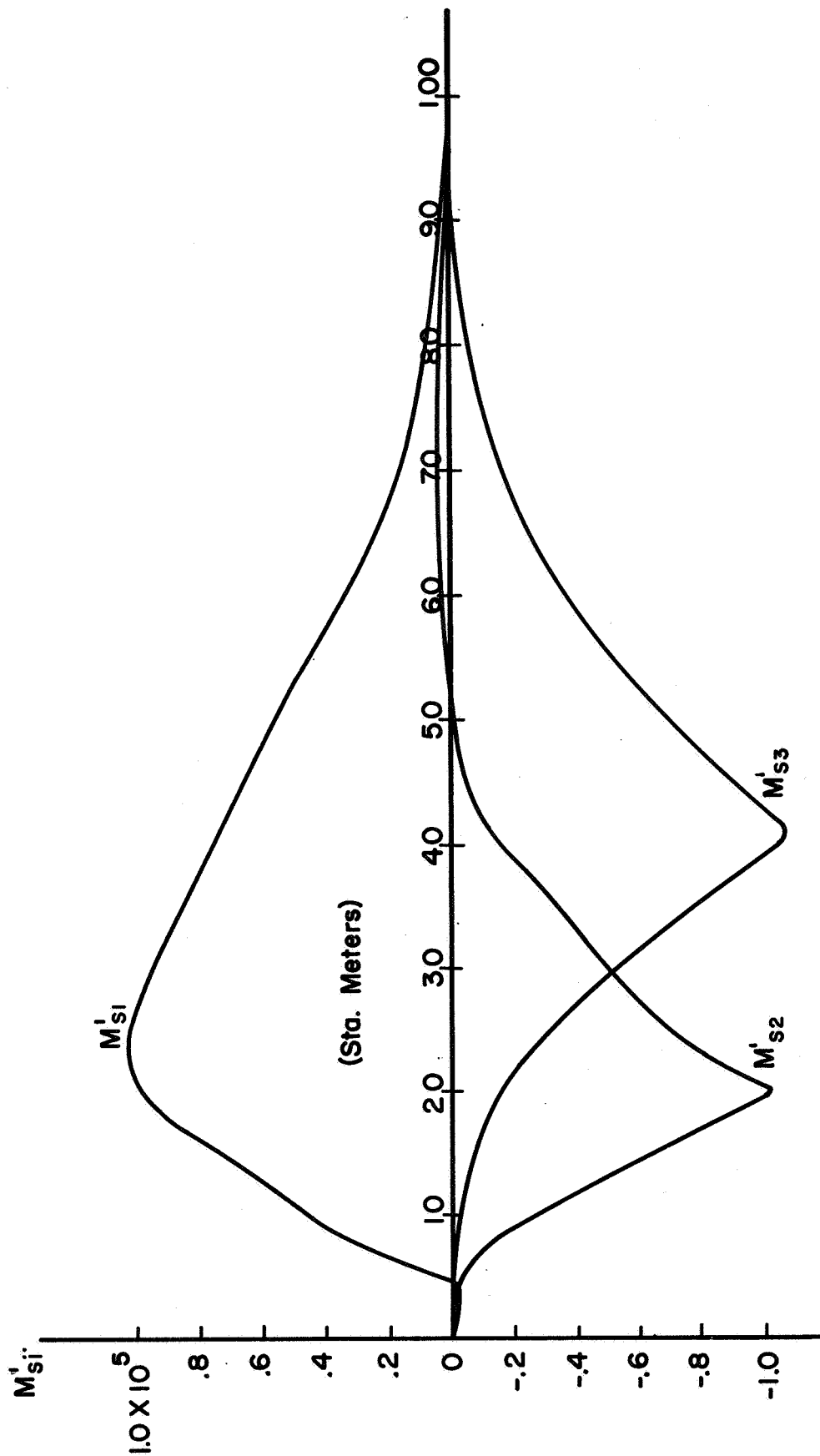


FIG. 3 BENDING MOMENT COEFFICIENT FOR SLOSHING DYNAMICS

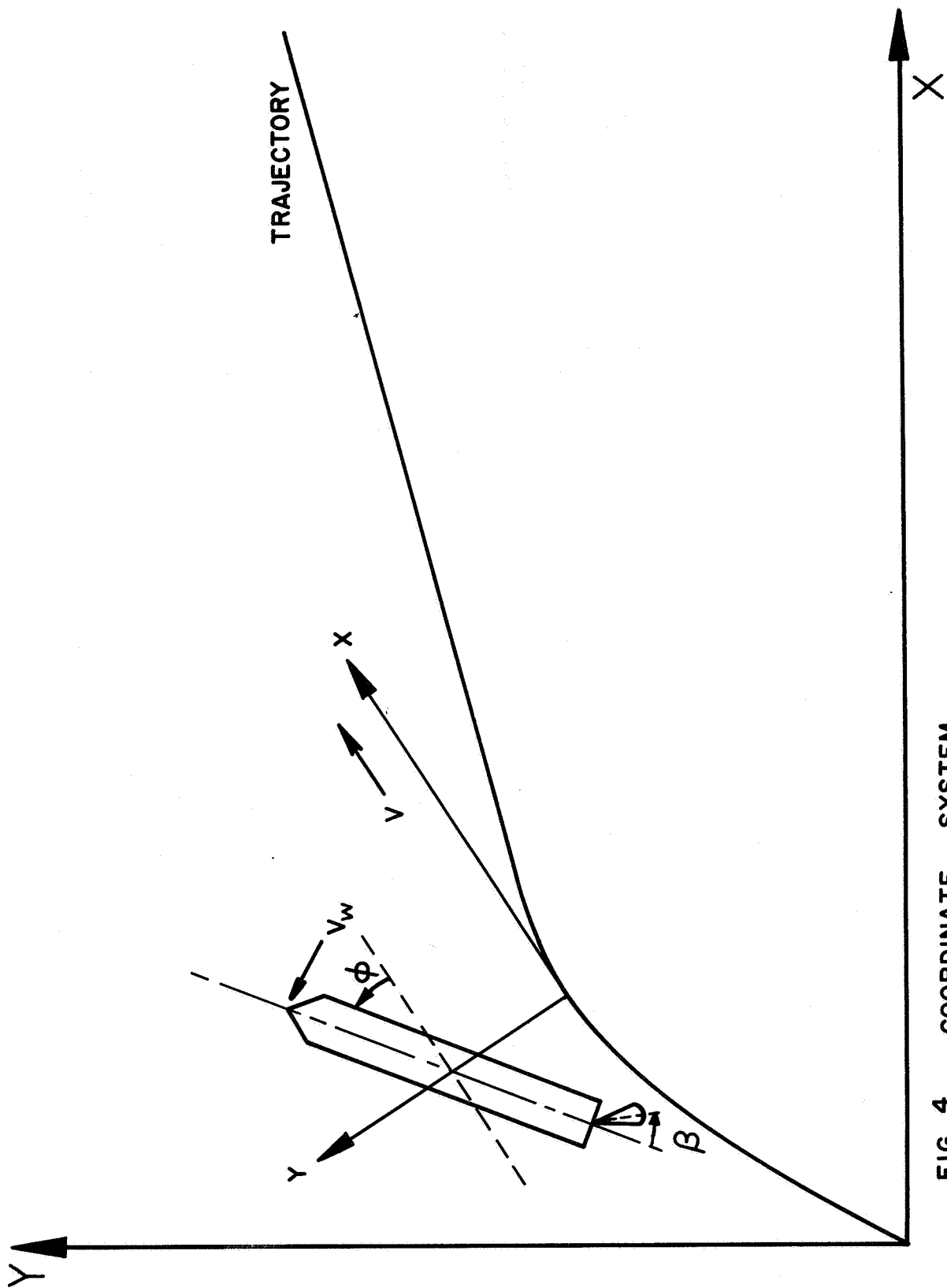


FIG. 4 COORDINATE SYSTEM

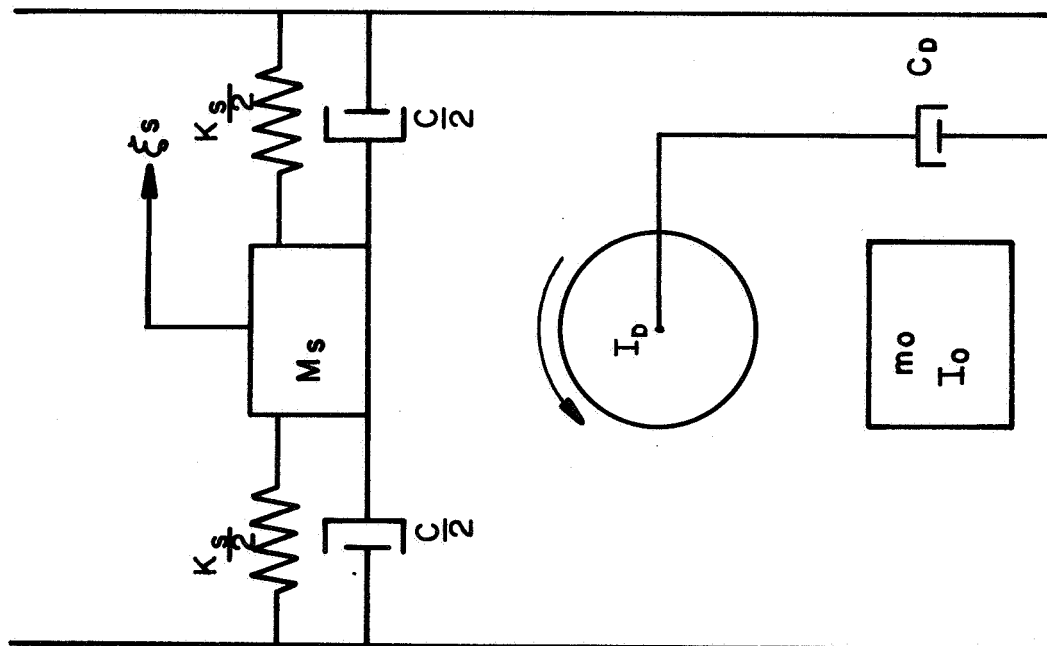


FIG. 5 SLOSH MODEL

$$\omega_s^2 = \frac{\xi_n}{a_f} - \bar{g} \tanh \xi_n \frac{h_f}{a_f}$$

$$M_s = \frac{2 \tanh \xi_n \frac{h_f}{a_f}}{\xi_n \frac{h_f}{a_f} (\xi_n^2 - 1)} M_f$$

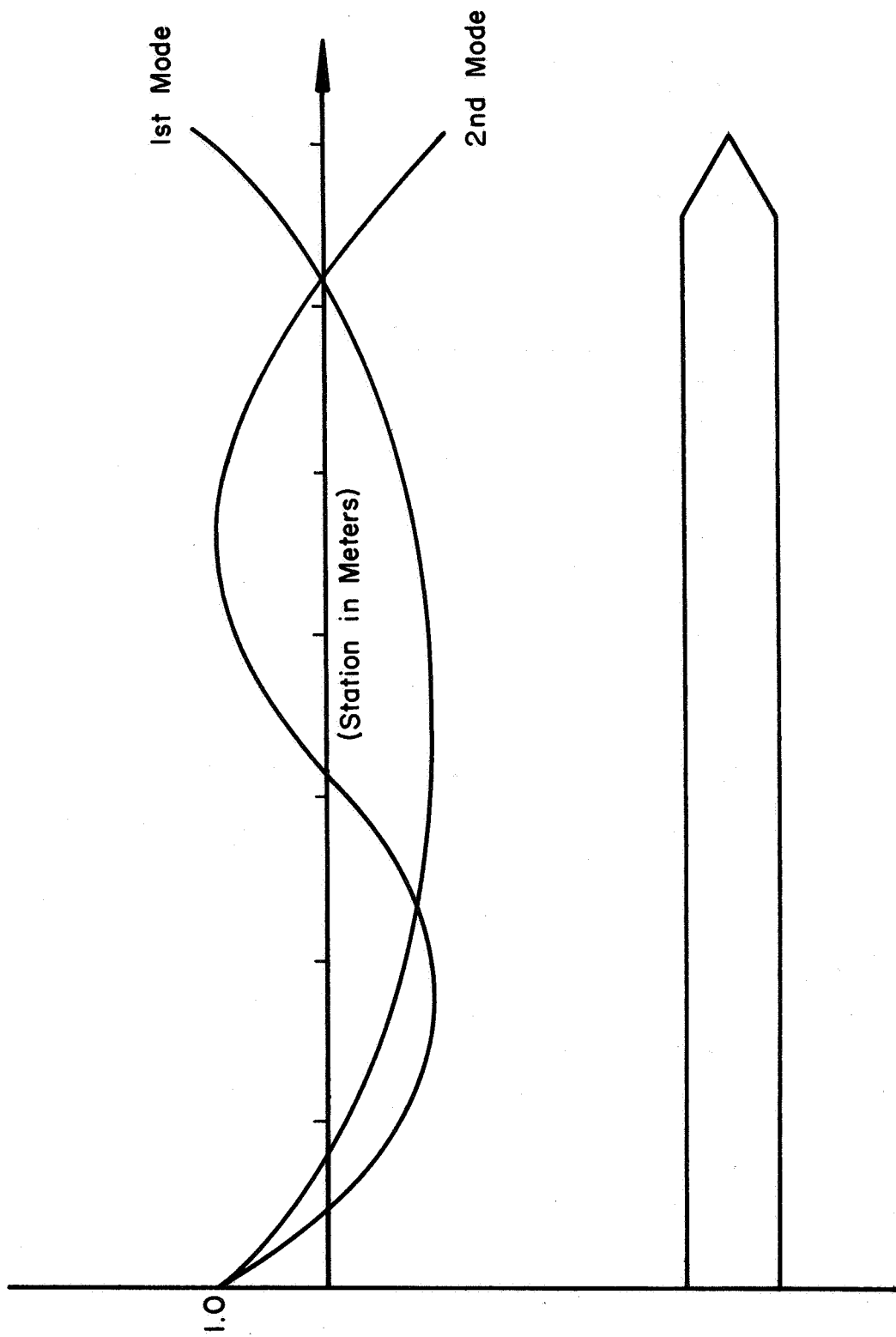


FIG. 6 BENDING MODE DEFLECTION CURVES

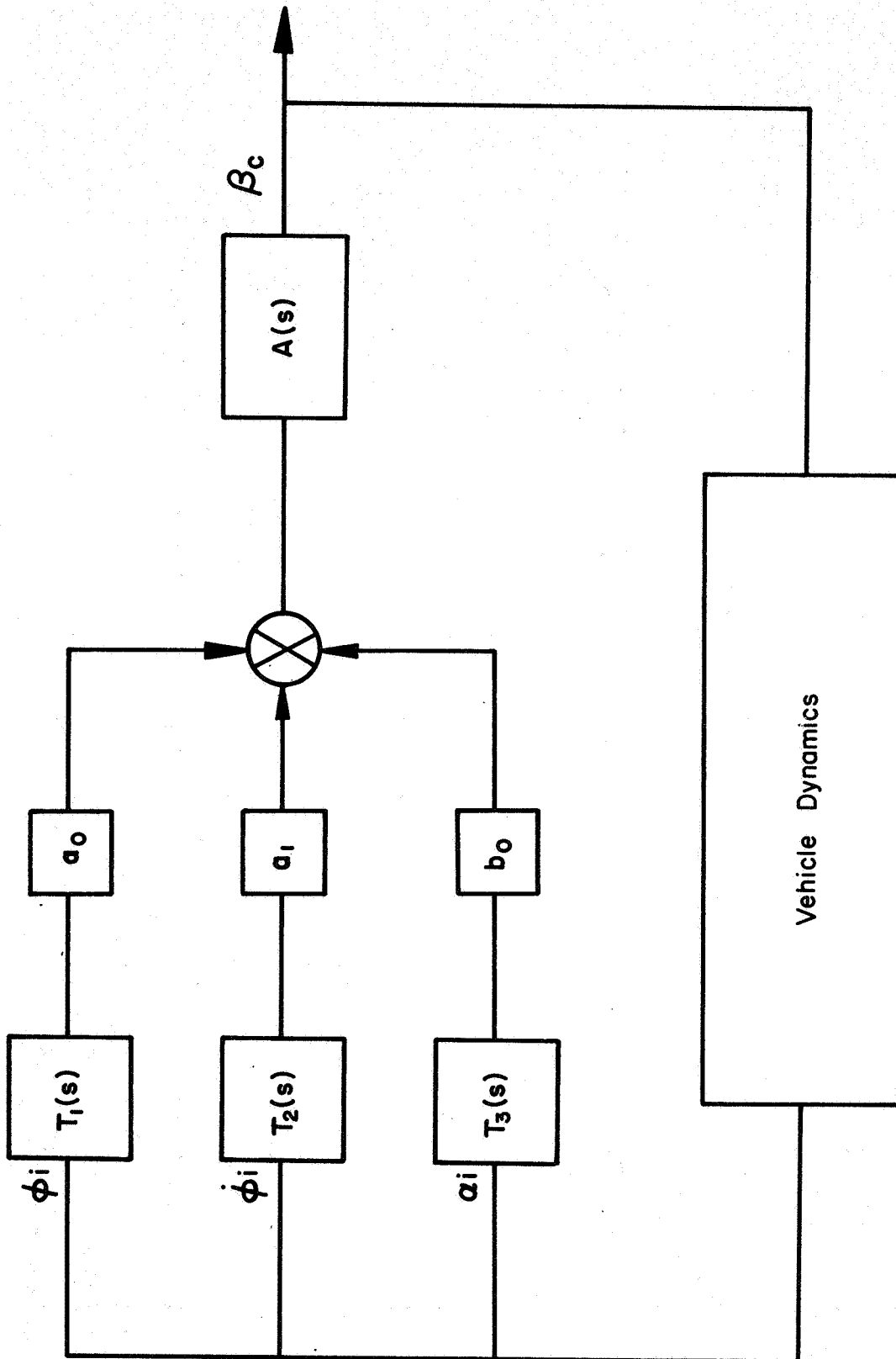


FIG. 7 CONTROL SYSTEM BLOCK DIAGRAM

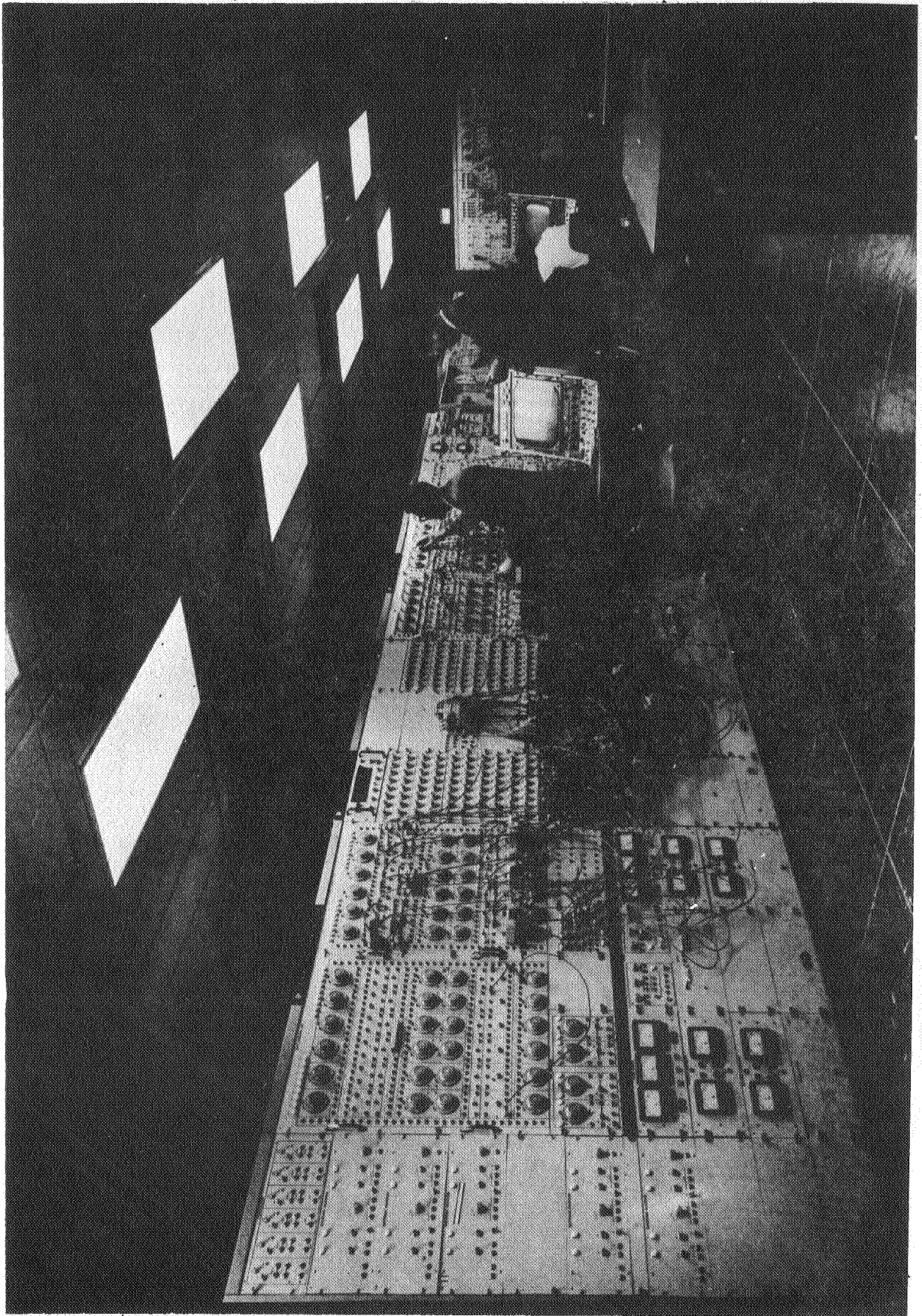


FIGURE 8. COMPLETE GPS FACILITY

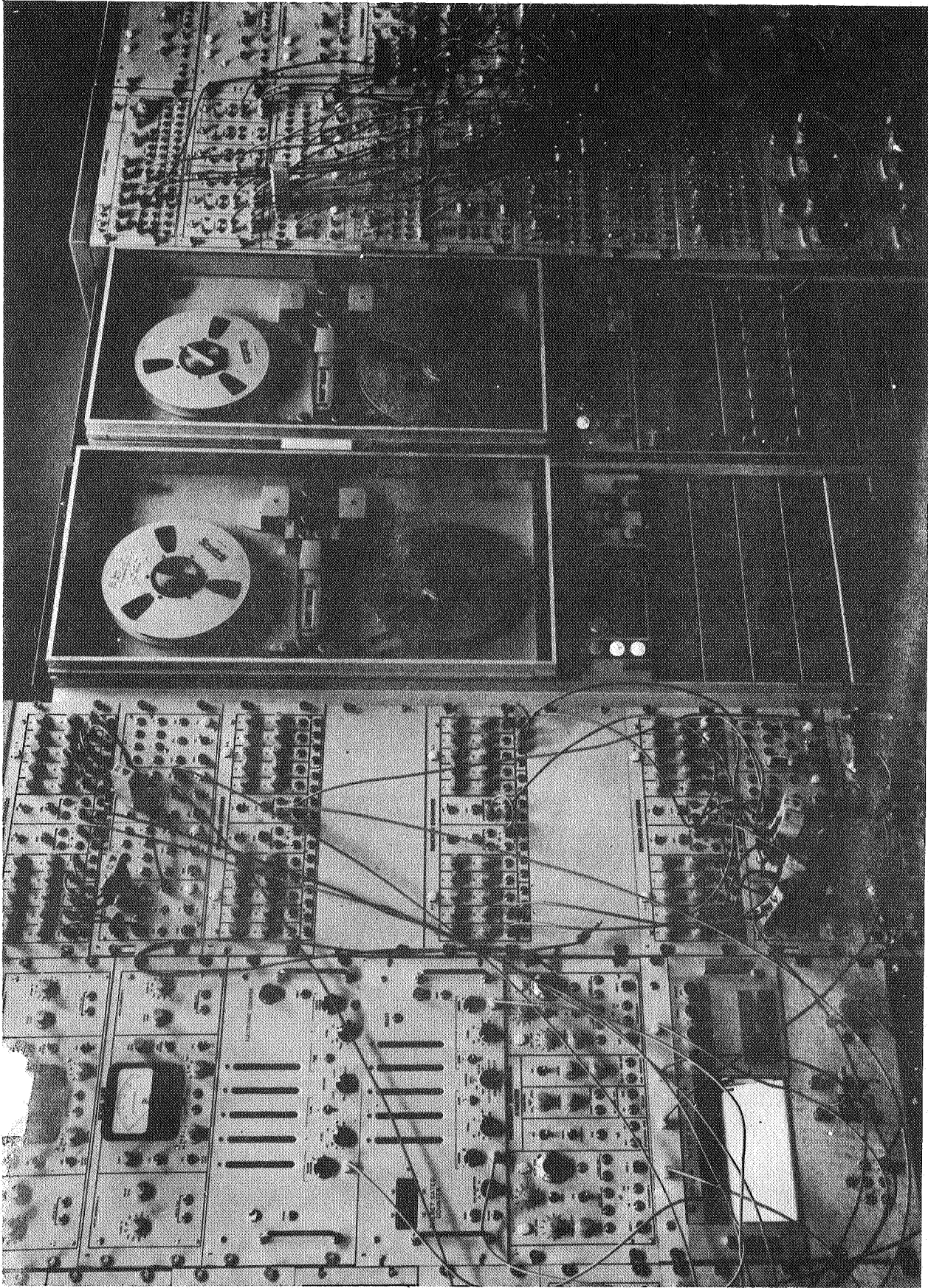


FIGURE 9. DETAILS OF THE COMPUTER

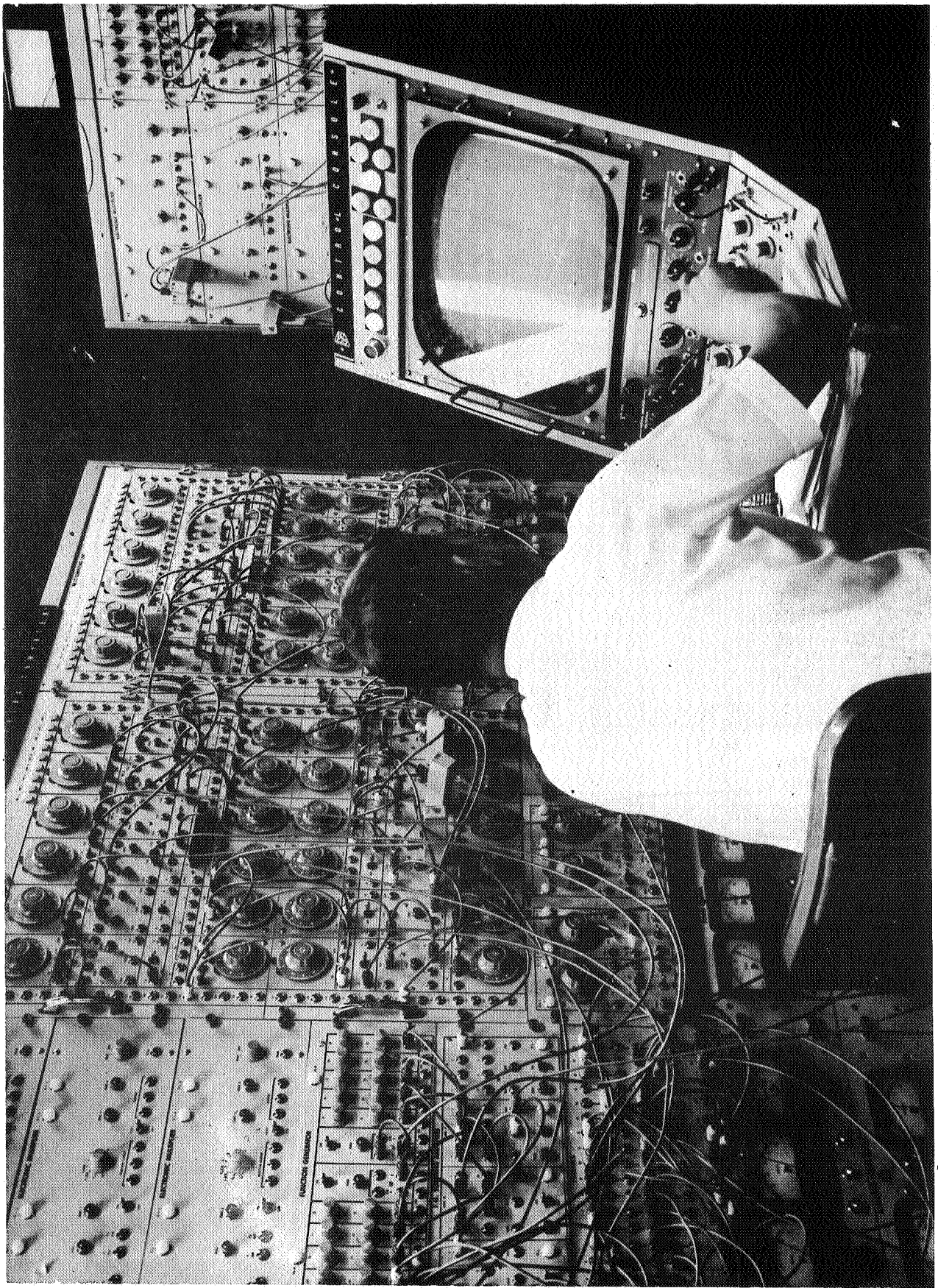


FIGURE 10. DETAILS OF THE COMPUTER



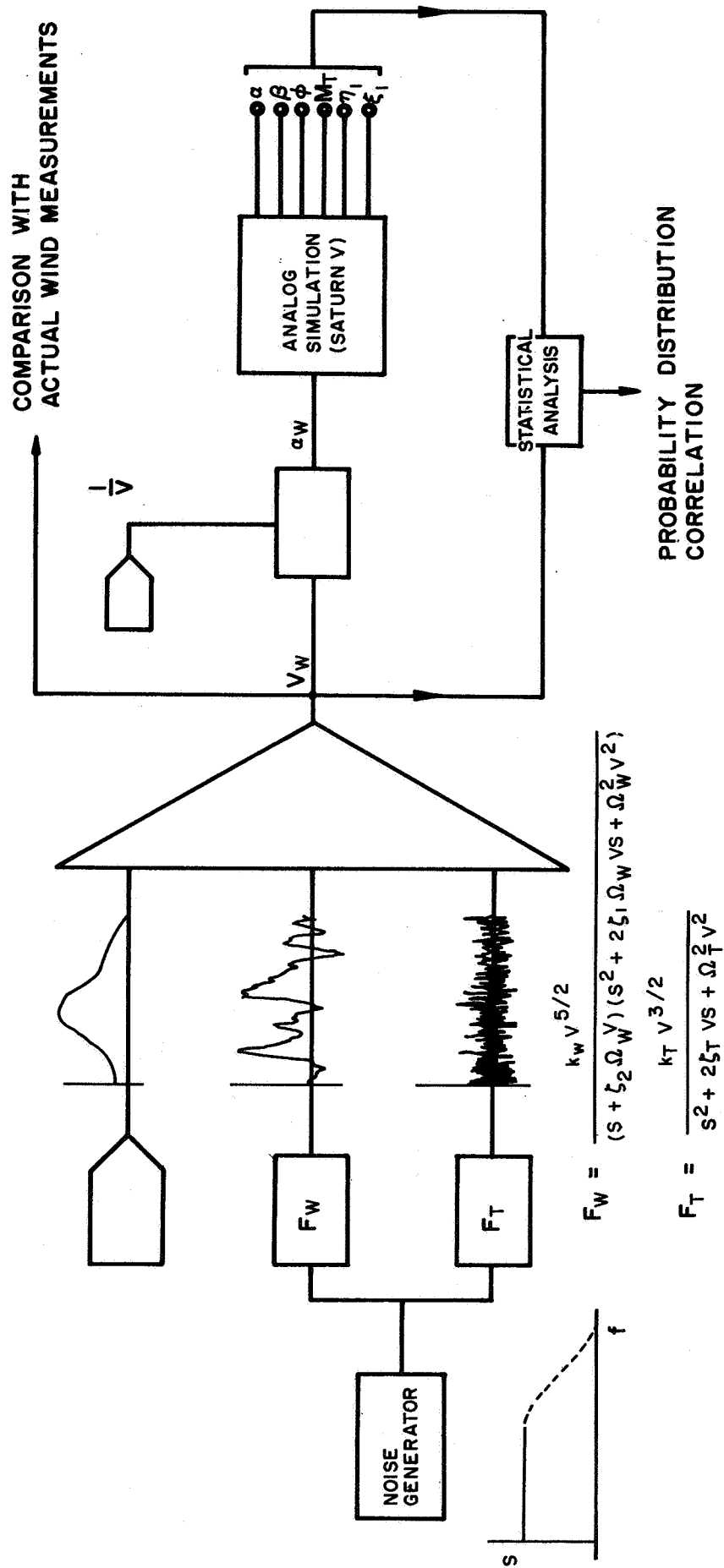


FIG. 13 SCHEMATIC FOR THE ANALOG SIMULATION OF WIND PROFILES

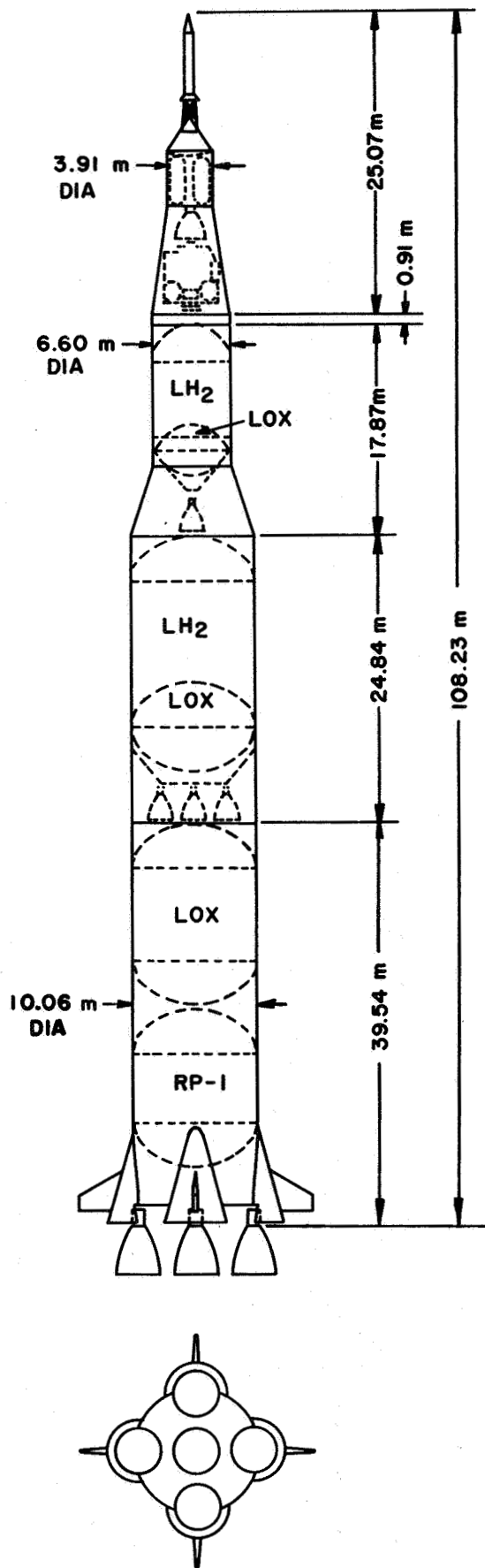


FIG. 14 SATURN V CONFIGURATION

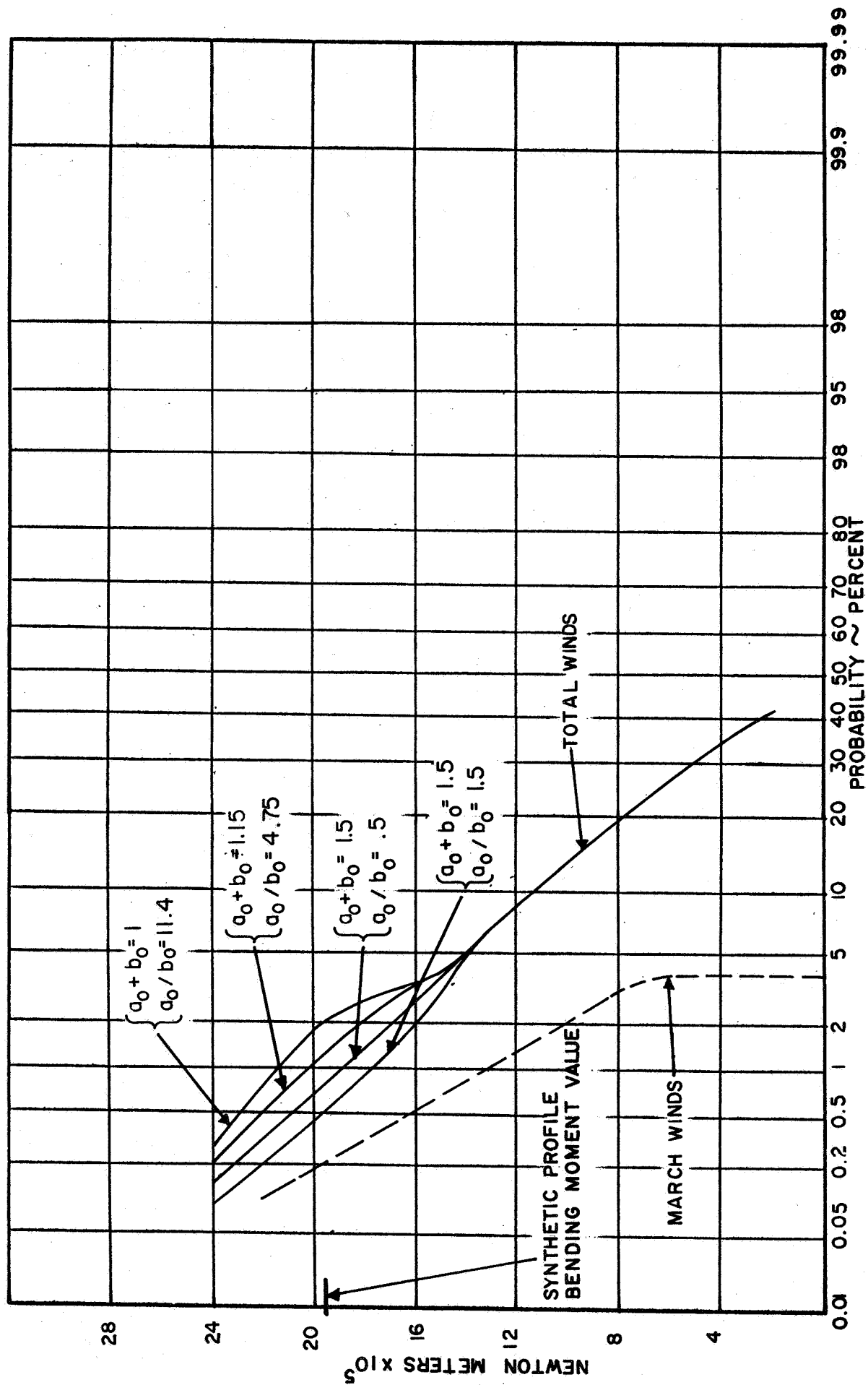


FIG. 15 BENDING MOMENT VS. PROBABILITY OF EXCEEDANCE

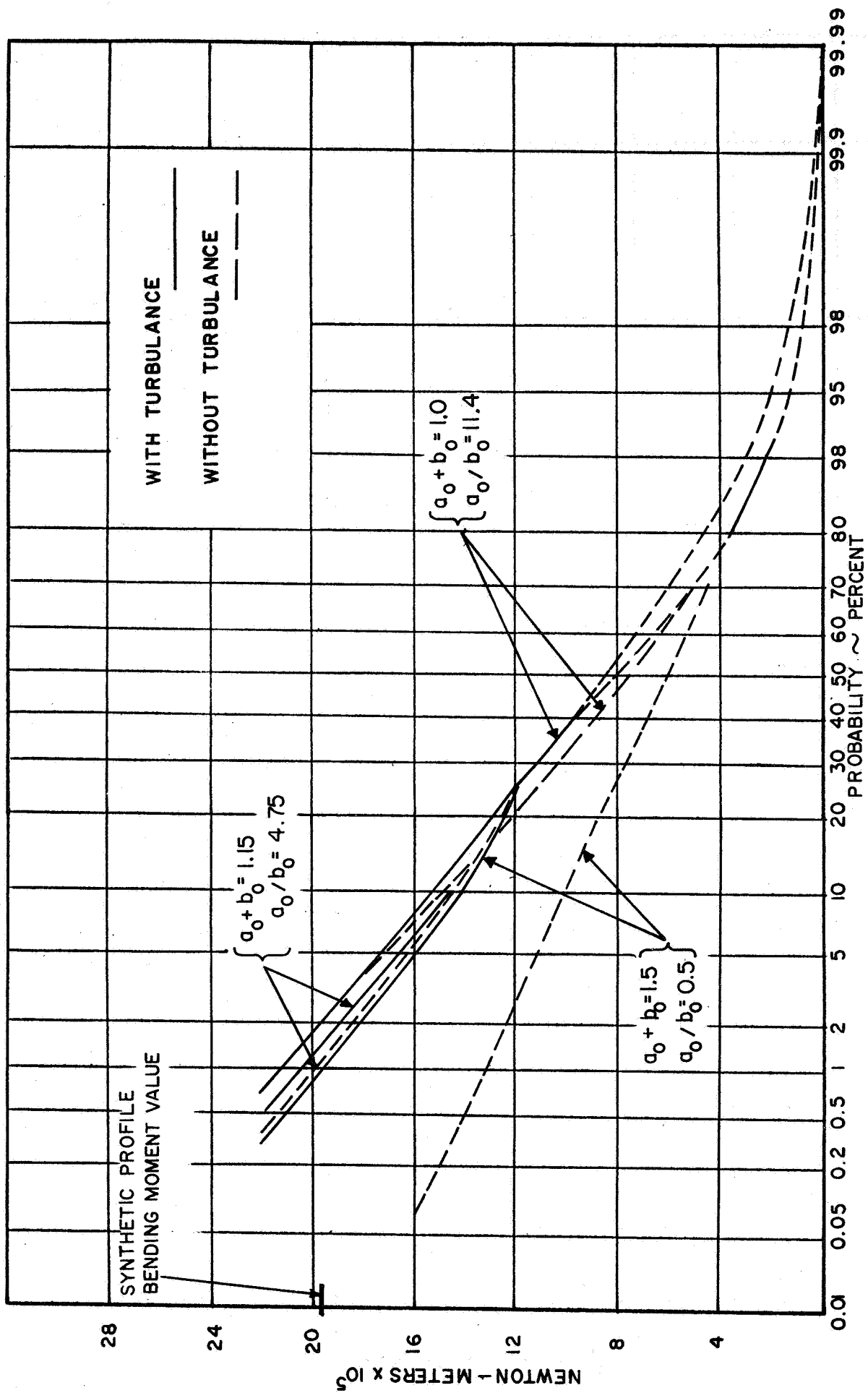


FIG.15A BENDING MOMENT VS. PROBABILITY OF EXCEEDANCE

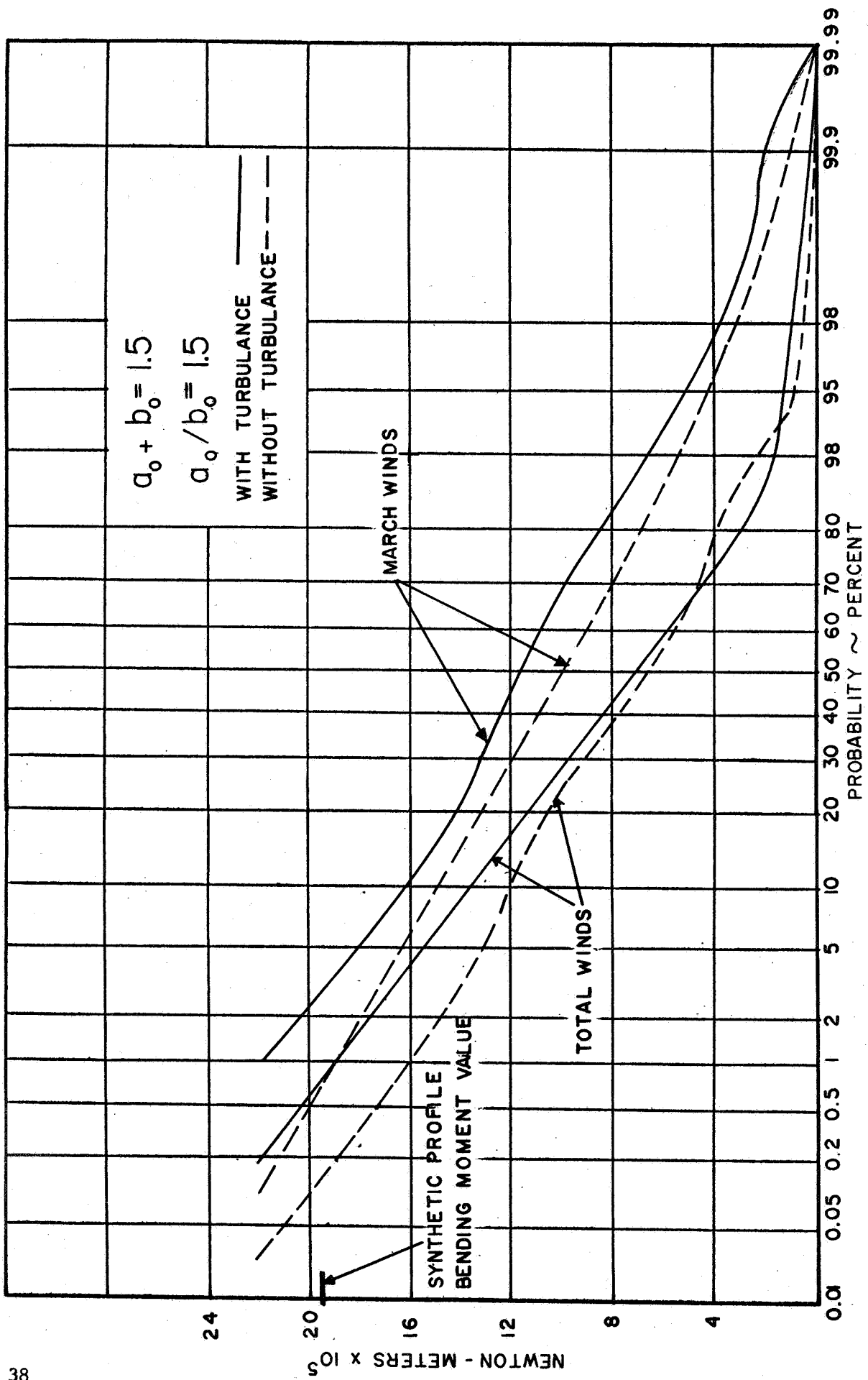


FIG. 15B. BENDING MOMENT VS. PROBABILITY OF EXCEEDANCE

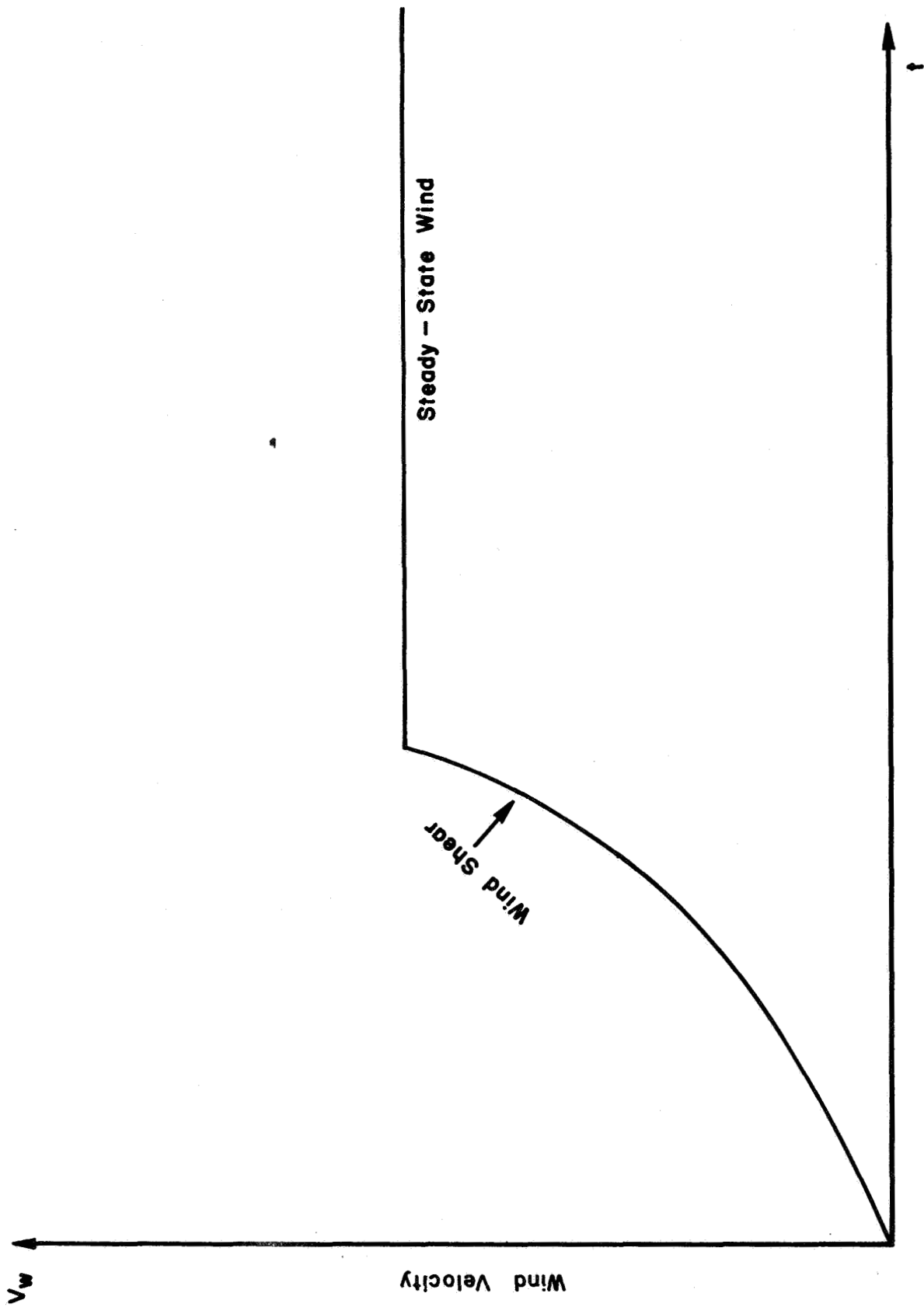


FIG. 16 MSFC SYNTHETIC PROFILE

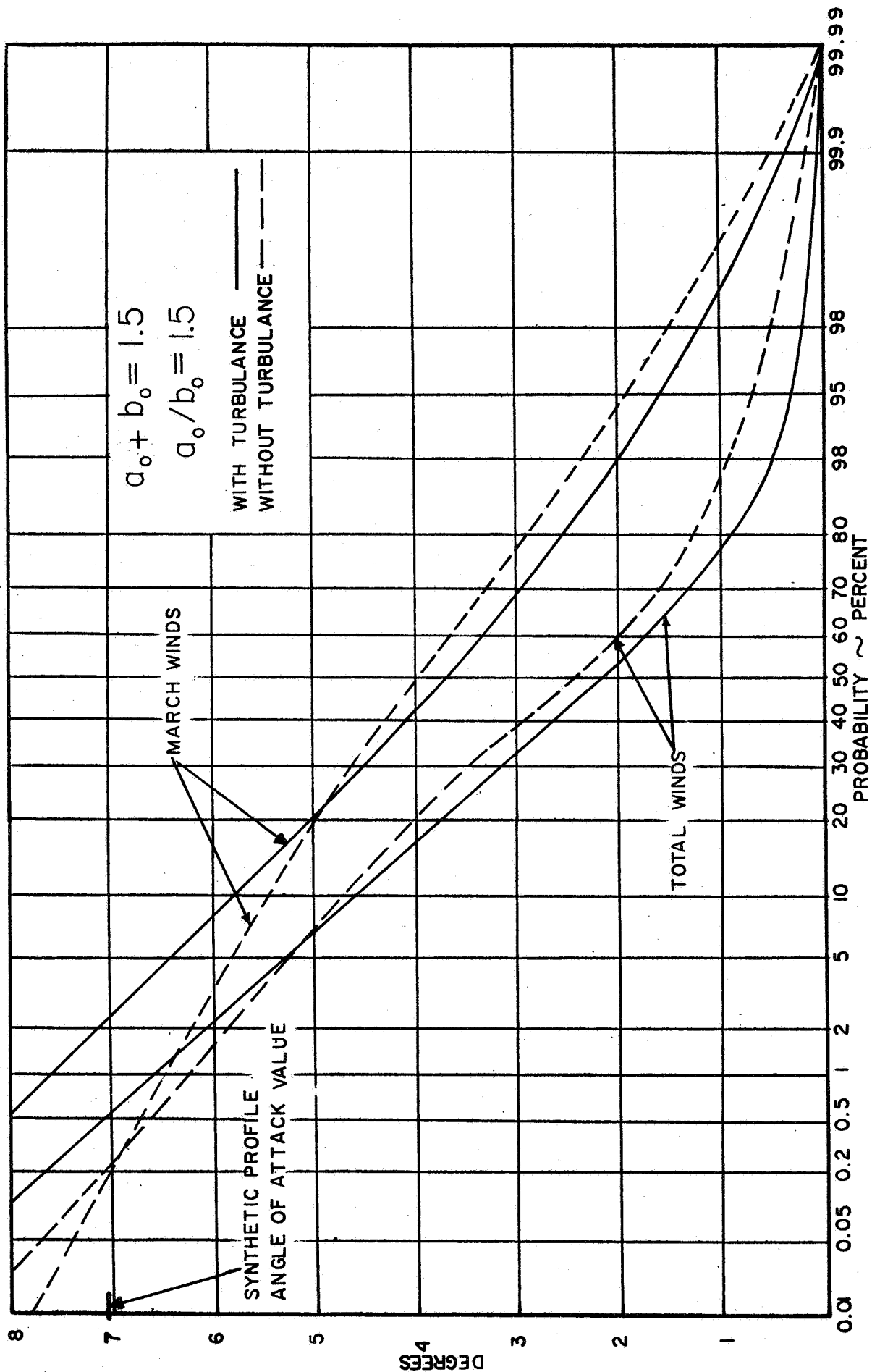


FIG. 17 ANGLE OF ATTACK VS. PROBABILITY OF EXCEEDANCE

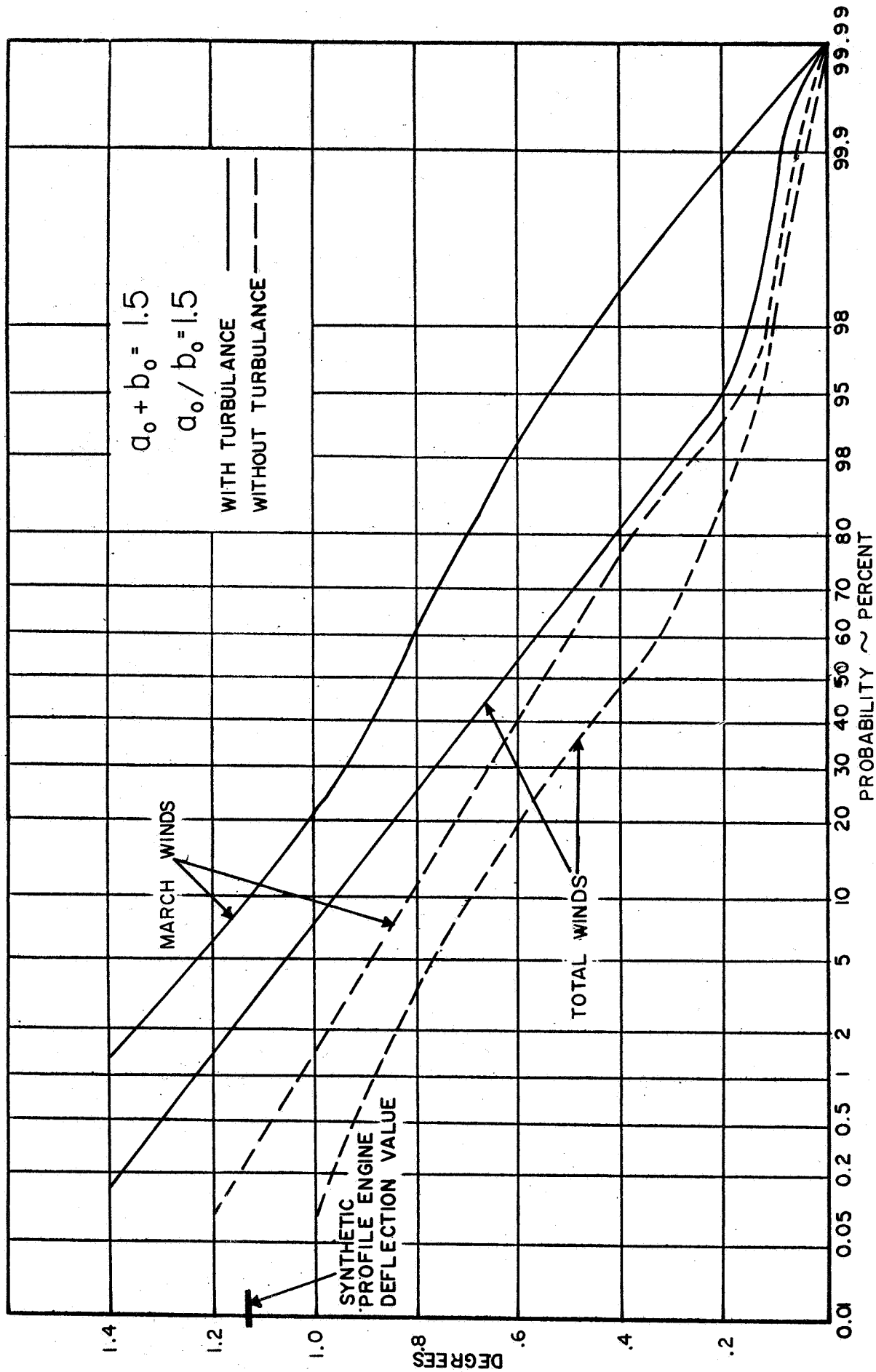


FIG. 18 ENGINE DEFLECTION VS. PROBABILITY OF EXCEEDANCE

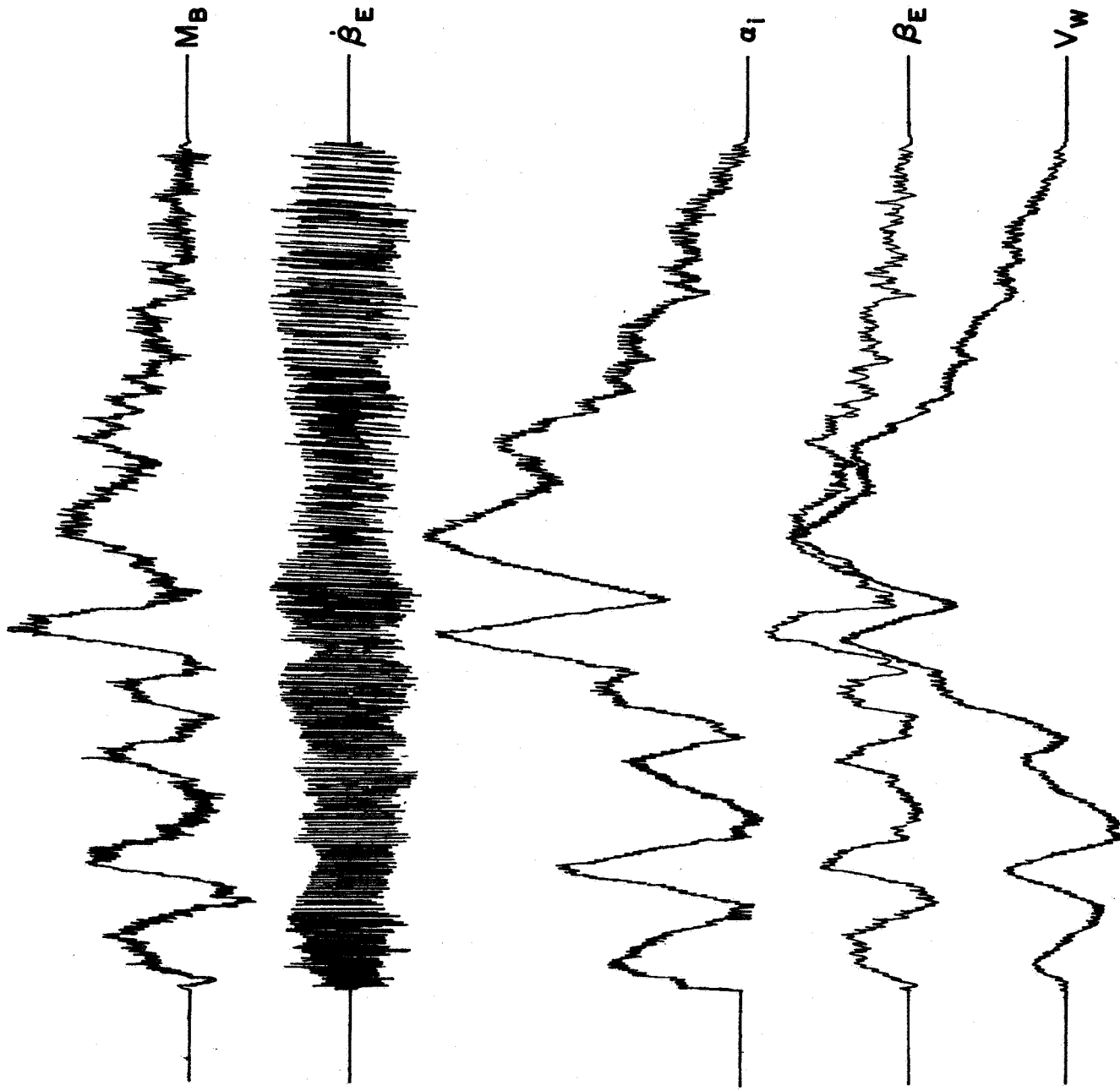


FIG. 19 TYPICAL RESPONSE WITH TURBULENCE

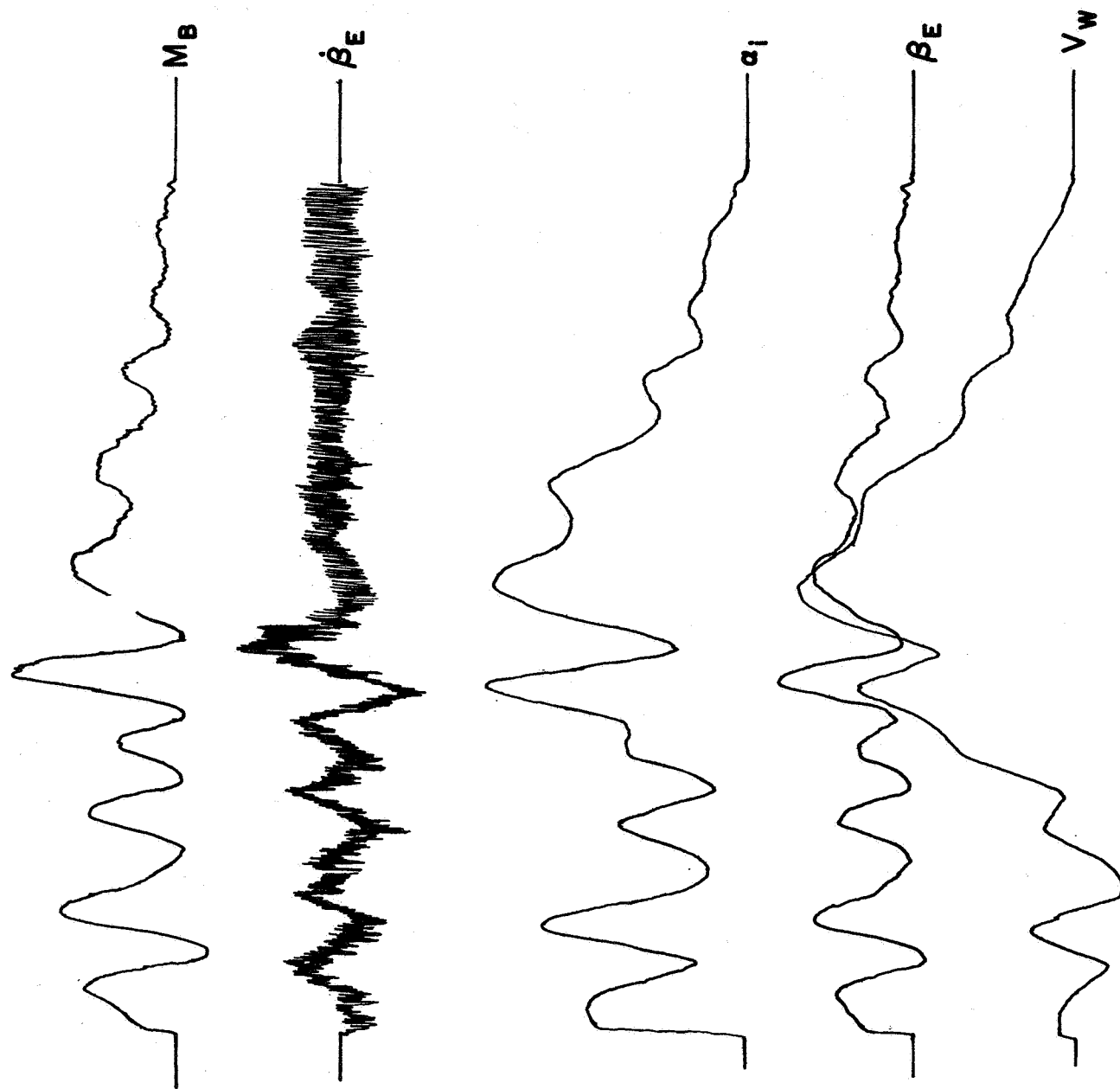


FIG. 19A TYPICAL RESPONSE WITHOUT TURBULENCE

APPROVAL

NASA TM X-53298

A PRACTICAL APPROACH TO THE OPTIMIZATION OF THE SATURN V
SPACE VEHICLE CONTROL SYSTEM UNDER AERODYNAMIC LOADS

By Robert S. Ryan and Dieter Teuber

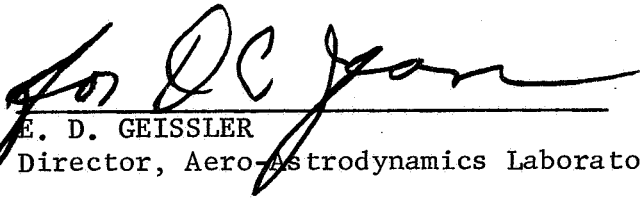
The information in this report has been reviewed for security classification. Review of any information concerning Department of Defense or Atomic Energy Commission programs has been made by the MSFC Security Classification Officer. This report, in its entirety, has been determined to be unclassified.

This document has also been reviewed and approved for technical accuracy.



HELMUT J. HORN

Chief, Dynamics and Flight Mechanics Division



E. D. GEISSLER

Director, Aero-Astrodynamic Laboratory

DISTRIBUTION

DIR

DEP-T

R-ASTR

Dr. Haeussermann
Mr. Hosenthien
Mr. B. Moore
Mr. Blackstone
Mr. George
Mr. Asner
Mr. Clarke

R-P&VE

Mr. Hellebrand
Mr. Hunt
Mr. Bullock
Mr. Showers
Mr. Sawyer
Mr. Beard
Mr. Sterett

MS-IP

MS-IL (8)

MS-T, Mr. Roy Bland (5)

MS-H

HME-P

CC-P

R-AERO

Dr. Geissler
Mr. Horn
Mr. Dahm
Dr. Speer
Mr. Ryan
Mr. Rheinfurth
Mr. Baker
Mr. Lovingood
Dr. McDonough
Mr. Pack
Mr. Hagood
Mr. Lindberg

R-AERO (cont'd)

Mr. Hagood
Mr. Lindberg
Mr. Milner
Mr. Townsend
Mr. Swift
Mr. Hays
Mr. Snow
Mr. Worley
Mr. Stone
Mr. Sumrall
Mrs. King (15)
Mr. Billups
Mr. Beutjer
Mr. Thomae
Mr. Papadopoulos
Mr. Kiefling
Mr. Scoggins
Mr. Vaughan
Mr. Teuber (5)

Scientific & Tech Info Facility (25)
P. O. Box 5700
Bethesda, Md.
ATTN: NASA Rep. (S-AK/RKT)